BNL-98067-2012-JA

EVALUATION OF PRECIPITATION SIMULATED BY SEVEN SCMS AGAINST THE ARM OBSERVATION AT THE SGP SITE

H. Song[1*], W. Lin[1], Y. Lin[2], A. Wolf[3], R. Neggers[4],
L. J. Donner[2], A. Del Genio[5] and Y. Liu[1]

[1]Brookhaven National Laboratory, Upton, NY, USA
[2]Geophysical Fluid Dynamics Laboratory/NOAA, Princeton, NJ, USA
[3]Columbia University, New York, NY, USA
[4]Royal Netherlands Meteorological Institute, De Bilt, Netherlands
[5]NASA Goddard Institute for Space Studies, New York, NY, USA
[*]Corresponding author: Brookhaven National Laboratory, Atmospheric Sciences Division, Bldg. 815E, 75 Rutherford Drive, Upton, NY 11973-5000; hsong@bnl.gov

Submitted to the Journal of Climate

May 2012

Atmospheric Sciences Division/Environmental Sciences Dept.

Brookhaven National Laboratory

U.S. Department of Energy
Office of Science

DISCLAIMER

Abstract

This study evaluates the performances of seven single column models (SCMs) by comparing simulated surface precipitation with observations at the Atmospheric Radiation Measurement Program Southern Great Plains (SGP) site from January 1999 to December 2001. Results show that although most SCMs can reproduce the observed precipitation reasonably well, there are significant and interesting differences in their details. In warm season, most SCMs produce more rain events in daytime than in nighttime while the observation has more rain events in nighttime. The mean intensities of rain events in most SCMs are much stronger (weaker) in daytime (nighttime) than the observation. In cold season, the model-observation differences in the frequency and mean intensity of rain events tend to compensate each other for most SCMs. In daytime, most SCMs have higher frequency of moderate-to-strong rain events than the observation in warm season. In nighttime, all the SCMs have lower frequency of moderate-to-strong rain events than the observation for both seasons. Diagnostic analysis reveals that the higher frequency of rain events during warm season daytime in most SCMs is related to the fact that most SCMs produce a spurious precipitation peak around the regime of weak vertical motions but large precipitable water and relative humidity. Further analysis of extreme events reveals distinct meteorological backgrounds for model underestimation and overestimation events. The model underestimation events occur in the strong ascending regimes with negative low-level horizontal heat and moisture advection whereas the model overestimation events occur in the weak (in daytime) or moderate (in nighttime) ascending regimes with positive low-level horizontal heat and moisture advection.

1. Introduction

Precipitation is one of the most poorly parameterized physical processes in numerical weather prediction and general circulation models (GCMs). While the double intertropical convergence zone (ITCZ) phenomenon is probably the most outstanding problem confronting GCMs for properly simulating the precipitation climatology (Lin 2007), there are even long-standing challenges for GCMs to simulate precipitation features as fundamental as the diurnal variation, and the frequency and intensity associated with individual weather systems. For example, most GCMs exhibit substantial biases in simulating the diurnal cycle of warm season precipitation: producing too much precipitation in the daytime but too little precipitation in the nighttime over land, and wrong timing of convective precipitation events as well (e.g., Ghan et al. 1996; Dai 2006; Lee et al. 2007; Lee and Schubert 2008). It is also common that models substantially overestimate the frequency of light precipitation and underestimate the intensity and/or frequency of heavy precipitation (e.g., Dai and Trenberth 2004; Sun et al. 2006). Even without considering the inevitable influence on the atmospheric circulation, the sheer bias in simulating the probability distribution of precipitation should cast doubt on the model's capability to predict high impact hydrological events.

One of the difficulties with modeling precipitation stems from the fact that in addition to large-scale circulation, precipitation is affected by a variety of complex processes that needs to be parameterized in large scale models, for example, deep convection, planetary boundary layer processes, and cloud microphysics (Dai 2006). It is not trivial to identify deficient aspects of the parameterizations, and many approaches have been proposed for this purpose. One of the commonly used approaches is to perform and evaluate simulations of corresponding single column models driven by the same large scale forcing (e.g., Randall et al. 2003; Neggers et al. 2012).

The SCM approach is also a key strategy of the US Department of Energy's Atmospheric Radiation Measurement (ARM) and Atmospheric System Research (ASR) programs (Stokes and Schwartz 1994; Ackerman and Stokes 2003). ARM organized several SCM intercomparisons using surface observations at the ARM sites. However, most of the previous studies have been focused on special cases, or week-to-month-long periods (e.g., Ghan et al. 2000; Xie et al. 2002; Xie et al. 2005), often limited by the large scale forcing needed to drive the SCM simulations and adequate evaluation data. Xie et al. (2004) have constructed multiyear (1999-2001) continuous large-scale forcing data over the SGP site using an objective variational analysis method constrained by surface and top-of-the-atmosphere observations. Together with other observations, the multi-year continuous large scale forcing data permit long-term SCM-based evaluation of the parameterized physics with much improved statistics. Kennedy et al. (2010) have lately evaluated the GISS SCM simulated clouds by taking advantage of the three-year large forcing data. Driven by these observationally constrained continuous large-scale forcing data, we have further carried out three year (1999-2001) SCM simulations of seven GCMs participating in the FAst-physics System TEstbed and Research (FASTER) project at the ARM SGP site, with the aid of the FASTER SCM testbed. Detailed information on the FASTER project and the testbed can be found at http://www.bnl.gov/esm/.

This study focuses on the statistical aspects that bear relevance to main existing issues of precipitation simulation (e.g., diurnal cycle, seasonal variation, convective/stratiform partitioning), including differing model biases in frequency and mean precipitation intensity between daytime and nighttime, between warm and cold seasons, and between convective and stratiform partition. In addition, we also attempt to demonstrate the relationship between surface precipitation and vertical pressure velocity, precipitable water and relative humidity, and to

investigate the large-scale backgrounds against which the model biases occur through the studies of extreme events.

The rest of the paper is organized as follows: Section 2 describes the model and data used in this study. The main results are presented in sections 3 and 4. Section 5 summaries the major results.

2. Model Description and Evaluation Data

2.1. Participating models

Three main US GCMs — the National Center for Atmospheric Research (NCAR) Community Atmospheric Model (CAM), the Geophysical Fluid Dynamic Laboratory (GFDL) Atmospheric Model (AM), the Goddard Institute for Space Studies (GISS) Model E2, and one European GCM — the European Centre for Medium-Range Weather Forecast (ECMWF) Integrated Forecast System (IFS) are participating the FASTER project. To further enhance the parameterization diagnosis and track the model improvement, the NCAR CAM and GFDL AM also include multiple versions (CAM3, CAM4 and CAM5; AM2 and AM3). Note that the GFDL AM3 here is not the full version of GFDL AM3 (Donner et al. 2011), which uses 48 vertical levels with aerosol activation (double moment for cloud droplets) and comprehensive chemistry. The AM3 here is close to the AM2 with the same vertical levels and cloud scheme. The major change of the AM3 from the AM2 is the convection scheme. The AM2 uses the relaxed Arakawa-Shubert scheme (Moorthi and Suarez 1992) for both deep and shallow convections while the AM3 uses the Donner cumulus scheme (Donner et al. 2001; Donner et al. 2010) for deep convection and University of Washington (UW) scheme (Zhao et al. 2009) for shallow convection. Table 1 lists the seven GCMs used in the intercomparison study, their precipitation-related parameterization schemes, the corresponding references, and their SCM resolutions. All the deep convection schemes of the seven GCMs are based on the mass flux approach, with some differences in the

closure assumptions, trigger mechanisms and formulations for convective updrafts and downdrafts. Previous studies show that the deficiency in convective trigger mechanism is one of the major reasons for different timing of precipitation occurrences (e.g., Xie and Zhang 2000; Betts and Jakob 2002; Zhang 2003; Bechtold et al. 2004; Lee et al. 2008). There are four kinds of convection triggers in the seven GCMs: CAPE threshold triggers for the GFDL AM3 and NCAR CAM3; cloud work function threshold trigger for the GFDL AM2; dilute CAPE threshold triggers for the NCAR CAM4 and CAM5; and parcel-lifting-based trigger for the GISS and ECMWF models. Dilute CAPE and cloud work function for entraining clouds are closely related, though the quantitative values of entrainment may vary widely. The SCM intercomparison study of Xie et al. (2002) indicates that the models using CAPE-only triggers generally produce the least agreement with the observation in surface precipitation. More information on the deep convection schemes and cloud microphysical schemes can be found in Xie et al. (2002) and the related references given in Table 1.

2.2 Model configuration and setup

The basic thermodynamic configuration for the SCM consists of two prognostic equations about temperature (T) and specific humidity (q):

$$\frac{\partial \bar{T}(p,t)}{\partial t} = -\vec{\bar{v}} \cdot \nabla \bar{T} - \bar{\omega}\frac{\partial \bar{T}}{\partial p} + \frac{\bar{\omega}}{c_p}\alpha + P_T + \frac{\bar{T}_{obs} - \bar{T}}{\tau_a}$$

$$\frac{\partial \bar{q}(p,t)}{\partial t} = -\vec{\bar{v}} \cdot \nabla \bar{q} - \bar{\omega}\frac{\partial \bar{q}}{\partial p} + P_q + \frac{\bar{q}_{obs} - \bar{q}}{\tau_a}$$

where the overbar denotes large (model grid) scale mean, $\vec{\bar{v}}$ is the large-scale horizontal wind velocity, $\bar{\omega}$ is the large-scale vertical pressure velocity, the terms $-\vec{\bar{v}} \cdot \nabla \bar{T}$ and $-\vec{\bar{v}} \cdot \nabla \bar{q}$ are the large-scale horizontal advection tendency terms, $-\bar{\omega}\frac{\partial \bar{T}}{\partial p}$ and $-\bar{\omega}\frac{\partial \bar{q}}{\partial p}$ are the large-scale vertical

advection tendency terms, α is the specific volume, P_T and P_q are the parameterized physics tendency terms, $\frac{\bar{T}_{obs}-\bar{T}}{\tau_a}$ and $\frac{\bar{q}_{obs}-\bar{q}}{\tau_a}$ are the relaxation terms, $\bar{T}_{obs}$ and $\bar{q}_{obs}$ are the observed values of T and q respectively, and τ_a is the relaxation timescale, which is set to 3 hours based on previous studies (e.g., Hack and Pedretti 2000).

Since SCMs do not predict the interaction with the environment outside of the target column, nor do they predict the vertical motion within the column, both the large-scale horizontal and vertical advection tendencies, along with surface forcings, are prescribed using the ARM variational analysis product (Xie et al. 2004). The variational analysis product was generated by constraining the National Oceanic and Atmospheric Administration rapid update cycle (RUC-2) analyses with ARM surface and top-of-the-atmosphere measurements.

The relaxation terms relax the simulated T and q toward the observations at each time step. They are unphysical and may appear to hide the errors in model physics (Ghan et al. 1999). However, Randall and Cripe (1999) found that error in SCM is conserved and use of relaxation does not hide model problems. Relaxation can also suppress the model's sensitivity to initial condition (Hack and Pedretti 2000) and act to adaptively correct the error in large-scale forcing. Precipitation in SCM is strongly constrained by the forcing. When the SCM is simply forced with the continuous large-scale forcing, the simulated precipitation cannot stray too far from the observed precipitation, even when the model thermodynamic state has large accumulated biases (e.g., Randall and Cripe 1999; Hack and Pedretti 2000). This would render the SCM framework ineffective in evaluating the underlying precipitation physics. Use of relaxation under such circumstances serves to unlock the strong link between large-scale forcing and precipitation.

For the three-year simulations from January 1999 to December 2001, all the seven SCMs are re-initialized at the beginning of each month and integrate for each whole month. The seven SCM outputs are averaged over 1 hour to match the temporal resolution of evaluation data (see Table 1 for the original SCM temporal resolutions).

2.3. Evaluation data

The precipitation data used in this study for evaluation are the SGP domain-averaged surface precipitation rates included in the continuous forcing data derived by Xie et al. (2004). They are the hourly Arkansas-Red Basin River Forecast Center (ABRFC) 4km rain gauge adjusted WSR-88D radar measurements averaged over the variational analysis domain.

Fields of vertical pressure velocity, specific humidity, relative humidity, horizontal thermal advection, horizontal moisture advection, surface latent heat (LH) flux and sensible heat (SH) flux in the continuous large-scale forcing data (Xie et al. 2004) are also used in this study.

3. Results

3.1. Frequency distribution of model bias

To investigate the capability of SCMs to reproduce the observed precipitation at different precipitation intensity, we first analyze the difference of precipitation intensity between the SCMs and observation. Precipitation at the SGP site has strong seasonal and diurnal variations, and many models (both GCM and SCM) cannot produce the observed diurnal variation of precipitation in the warm season (e.g., Bechtold et al. 2004; Xie and Zhang 2000). To inspect these aspects with enough statistics, the data are further partitioned into daytime, nighttime, warm and cold seasons in the analysis.

Figure 1 shows the frequency distribution of the model-observation differences in total precipitation intensity for all-time, daytime and nighttime data, respectively. Here daytime is defined by the positive solar insolation larger than 0.01 W/m^2 (otherwise nighttime). Several points are evident. First, mostly the absolute model biases are less than 1mm/day. Second, the SCMs underestimate the observed precipitation intensity more frequently than they overestimate. Third, while the frequencies of having large negative biases are comparable among the models, the likelihood of having large positive biases is much more distinguishable. Finally, large positive biases much more frequently happen in the daytime than in the nighttime, except for GISS and GFDL AM2 SCMs which have much fewer large overestimation events anyway.

The frequency distribution of the model biases in precipitation intensity for the warm season and cold season respectively are shown in Figure 2. Here the warm season is from May to October and the cold season is from November to April. It is seen that the frequencies of large precipitation biases, especially daytime overestimation events, are much higher in the warm season than in the cold season, implying that most SCMs perform better in the cold season than in the warm season. Again, there are very few overestimation events in the GISS and GFDL AM2 SCMs for both the warm and cold seasons. Figure 2 also reveals that the discrepancy in frequency of large positive biases among the models as seen in Figure 1 happens in the warm season.

The above analyses show that although all the seven SCMs can produce the observed precipitation reasonably well, they tend to underestimate the observed precipitation intensity more frequently, with striking differences between the daytime and nighttime, and between warm and cold seasons.

3.2. Frequency vs. precipitation intensity analyses

Total precipitation amount during a period can be expressed as a product of the number of all precipitation events and the mean precipitation intensity of all precipitation events during that period. Similarly, the bias in model precipitation may be attributed to precipitation intensity and/or frequency of precipitation events. This section examines the SCM performance from this perspective. Bias analysis of precipitation intensity and/or frequency may also shed light on deficiencies in the treatment of the underlying physical processes, particularly the relative roles of convective and stratiform precipitating processes in contributing to the total precipitation and its biases. It is noteworthy that while it is well-known that GCMs (e.g., Dai and Trenberth 2004) tend to overestimate frequency of light precipitation and underestimate the frequency of heavy precipitation, but in those unconstrained model simulations, the difference in simulated frequency occurrence of precipitating weather regimes and their maintenances could also be an important factor. Use of SCMs driven by the same observed large-scale forcings in this study minimizes the influences of potential biases from large-scale atmospheric and surface conditions.

Figure 3 compares the occurrence frequency and mean intensity of rain events in the 7 SCMs and observation for all-season, warm season and cold season, respectively. Here, a rain event is defined by the hourly surface total precipitation intensity larger than 0.1mm/day. In the observations, rain occurs about 28% of the time in both daytime and nighttime (Figure 3a). Compared with the observations, the three NCAR CAM SCMs (hereafter as SCAM3, SCAM4 and SCAM5, respectively) produce more rain events while the two GFDL AM and ECMWF SCMs produce much fewer rain events. Except for the GISS SCM, all the other six SCMs rain more frequently in the daytime than in the nighttime. Yet the mean hourly precipitation intensities in most SCMs are weaker than the observed especially in the nighttime. The observed mean precipitation intensity is stronger in the nighttime than in the daytime, which is opposite in

the GFDL AM3 and three NCAR SCAMs. The distributions of frequency and mean intensity for rain events in the warm season and cold season are quite different. In the warm seasons (Figure 3b), the three SCAMs have more rain events than the observation in the daytime but most SCMs have fewer rain events than the observation in the nighttime. Among the three SCAMs, nighttime precipitation frequency improves from SCAM3 to SCAM4 and SCAM5, but daytime overestimated precipitation frequency is biased further higher. In general, among the SCAMs, the higher the precipitation frequency a model has, the lower the mean precipitation intensity, suggesting some compensating errors between precipitation intensity and frequency in the SCAMs. The GISS and GFDL AM2 SCMs tend to underestimate both frequency and intensity in both daytime and nighttime, while the GFDL AM3 and ECMWF SCMs underestimate the frequency but overestimate the mean intensity in both daytime and nighttime. In the cold season (Figure 3c), the GISS SCM and three NCAR SCAMs have higher precipitation frequency but weaker precipitation intensity, compared to the observation, which is true for both daytime and nighttime conditions. The two GFDL and ECMWF SCMs have much lower frequency but stronger intensity than the observation in daytime.

The more detailed frequency distributions of the hourly precipitation intensity are shown in Figure 4. Overall, frequency of precipitation occurrence decreases with increasing precipitation intensity in both the observations and the models. The model bias characteristics however vary between different seasons and daytime or nighttime conditions. In warm season, compared with the observations, the nighttime frequencies for moderate to strong precipitation (Pr > 5 mm/day) are lower for all models, while daytime frequencies for stronger precipitation are mostly higher except for the GISS and GFDL AM2 SCMs. The frequencies of light precipitation (Pr < 1 mm/day) in warm season are higher only in GISS model and SCAM5, which is true for both daytime and nighttime conditions. In cold season, the light-to-moderate precipitation events (Pr

< 5 mm/day) occur more frequently in both daytime and nighttime for the GISS and three NCAR CAM SCMs. The two GFDL and ECMWF SCMs have a lower frequency occurrence for the entire precipitation spectrum. In addition, in the daytime, the GISS SCM has much higher frequency of precipitation events stronger than 1 mm/day in the cold season than in the warm season, while the observation and most other SCMs have higher frequency of mild-to-strong precipitation events (stronger than 1 mm/day and weaker than 50 mm/day) in the warm season than in cold season. Another noteworthy point is that the frequency differences between each SCM and observation are smaller in the cold season than in warm season for strong precipitation events (Pr>20 mm/day).

3.3. Partition between convective and stratiform precipitation

Modeled total precipitation is the sum of convective precipitation and stratiform precipitation from the convection scheme and large-scale macrophysical/microphysical schemes respectively. To examine the relative contributions of convective and stratiform precipitating processes to the total precipitation biases, Figure 5 shows ratios of the convective precipitation to total precipitation in the 7 SCMs at each specified total precipitation ranges, for warm season and cold season, respectively. In general, the relative contribution to total precipitation by model convective process is larger during the warm seasons and more so during the daytime than during the nighttime to some extent, though in the observation, if the frequency of stronger precipitation is any indication, there exists no such a tendency in either warm or cold seasons. For most SCMs the ratios of convective precipitation are larger in the daytime than in the nighttime.

It is also worth noting that the performances of the two GFDL SCMs are significantly different in that the AM2 SCM has much higher convective-to-total precipitation ratios in the rain events

weaker than 5 mm/day while the AM3 SCM has much higher convective-to-total precipitation ratios in the rain events stronger than 20 mm/day. The ratios of the convective precipitation to total precipitation in the three SCAMs are also quite different. The convective precipitation ratio is higher in SCAM3 and lower in SCAM5 especially in the nighttime. Other than GFDL AM2, the convective scheme in general has a relatively small role in light precipitation events, though the role is relatively larger for most models in the daytime and warm season. Under all conditions, the convection scheme in GISS model plays a much smaller role, compared to the other six models, in producing surface total precipitation. This will be further discussed later.

4. Further Analyses

4.1. Relationship between precipitation and possible influencing factors

The above analysis shows that although most models can reproduce the observed total precipitation reasonably well, there are significant and interesting differences in their details. This section examines possible factors that likely influence the detailed model performances.

Figure 6 compares the scatter-plots of 500-hPa vertical pressure velocity and total precipitation for rain events only. Total precipitation is tightly coupled to the large-scale vertical motion in the observations, especially in the warm season (Figures S1 and S2). The warm season also has more frequent extreme upward motions and precipitation in nighttime than in daytime. The close correlation between total precipitation and vertical motion may arise from the fact that the variational algorithm is constrained by surface precipitation. However, these two quantities are much less tightly coupled in the models and the relationship differs in different SCMs. Compared to the observation, there exists a significant precipitation bias in most models when vertical motions are weak, and the bias occurs predominantly in the daytime and in the warm season. It is interesting to note that GFDL AM3 SCM and SCAM3 still have some biases in the

cold season. On average, the model coupling between precipitation intensity and large-scale vertical motion is stronger in the cold season than in the warm season, even after excluding the large precipitation bias at the weak vertical motion regime. It is worth emphasizing that this seasonal difference is completely opposite to that in the observations. Compared to the other models, the GISS and GFDL AM2 SCMs do not exhibit a significant precipitation bias in the weak vertical motion regime.

Bretherton et al. (2004) showed a tight relationship between surface precipitation rate and precipitable water (vertically integrated specific humidity) over the tropical oceanic regions using the satellite data, and suggested that such a relationship can provide a useful constraint on the parameterization of tropical deep convection. To see if there is a certain relationship between the two variables in the observation over mid-latitude land and how well the models capture this relationship, here we analyze and compare the relationships between precipitation and precipitable water (PW) at the ARM SGP site in the observation and seven SCMs. Figure 7 depicts the averaged total precipitation, stratiform, and convective precipitation binned by PW in the daytime and nighttime, respectively. Total precipitation rates increase with PW in both the observations and the SCMs. However, the increase of precipitation with increasing PW levels off beyond PW ~ 20 mm in the observations in the daytime whereas GFDL AM3, ECMWF, and NCAR CAM3 SCMs do not capture this behavior. It is mainly due to the excessive precipitation from their convection schemes. Again the models have a better agreement with the observations during the nighttime. The primary contributor to the relationship is the convection-induced precipitation except for the GISS and NCAR CAM5, whose stratiform schemes play larger roles in accounting for this relationship.

To further investigate how the above-mentioned two possible influencing factors are related to precipitation, the joint probability distribution function (PDF) of 500hPa vertical pressure velocity and PW is shown in Figure 8 (shaded area), along with the averaged total precipitation intensity (contour) for each joint bin. It is clear that the most frequent events occur around the weaker vertical motion regimes with PW ranging from 10 mm to 50 mm. The frequency peak with larger PW occurs in the warm season and the peak with smaller PW occurs in the cold season (Figures 3S and 4S). On the other hand, PW also increases with the strengthening ascending velocity. In the observation, the increase of the averaged total precipitation intensity mostly coincides with the increasing vertical velocity, while in most SCMs except for the GISS and GFDL AM2 SCMs, stronger influence of PW is evident, indicated by the tilting of isopleths of 5 mm/day and 10 mm/day around the weak vertical motion regimes, especially in the daytime (Figures S5 and S6). This may be one of the reasons that the model precipitation is not coupled with the large-scale vertical motion as tightly as the observations shown in Figure 6. The model precipitation's stronger dependence on the PW is mostly due to the treatment of convective process, which is illustrated in Figure 7. The value of PW measures the total available water vapor in the whole air column; another moisture variable that is better related to condensation and conversion to precipitation is the air column relative humidity (hereafter as RH). The joint PDF (contour) for the column-averaged RH and PW in the weak vertical motion regimes (magnitudes of vertical pressure velocity are smaller than 50 hPa/day), and the averaged total precipitation (shaded area) for each joint bin are shown in Figure 9. The joint PDF demonstrates that the most frequent events are associated with column RH about 50% and PW about 40 mm in the observation and most SCMs. The precipitation intensity is quite small in the observation for all joint bins, while in most SCMs there are some intense rain in the events with large RH and PW, which is mostly contributed by the convective precipitation (Figure 10) in the daytime (Figures S7 and S8).

The analysis in this section shows that: (1) the large difference between the observation and SCM simulated precipitation is mainly around the weak vertical motion regimes. (2) Most SCMs produce strong precipitation (mainly from convective precipitation) when there are large PW and RH around the weak dynamical regimes, which is not seen in the observations. This difference implies that the observed surface precipitation at the SGP site is mainly controlled by large-scale vertical uplift, while the production of precipitation in most of the models from the cumulus/stratiform scheme may be more complicated and controlled by some other thermodynamic factors that affect PW and RH.

4.2. Analysis of extreme events

To further pin down the conditions under which the models tend to underestimate or overestimate the observed precipitation, a number of special events with substantial precipitation biases are selected. Particularly interesting are the two extreme categories of events: (1) all the SCMs underestimate the observed precipitation more than 20 mm/day, and (2) most SCMs overestimate the observed precipitation more than 10 mm/day (the events that SCMs overestimate the observed precipitation more than 20 mm/day are very few in the nighttime). Since there are very few overestimate events in the GISS and GFDL AM2 SCMs (Figure 1), there are no events that all the SCMs overestimate the observed precipitation simultaneously.

Figure 11 compares the total precipitation and convective precipitation rates for the two categories, in daytime and nighttime. For the category whereby all the SCMs underestimate precipitation, the total precipitation rates in the seven SCMs are quite similar in both daytime and nighttime, all being much weaker than the observation. For the category whereby some models overestimate by more than 10 mm/day, the events occur when the observation has weak

(daytime) or moderate (nighttime) precipitation. The convective precipitation rates are excessively large in most SCMs in the daytime.

Figure 12 further compares the profiles of averaged vertical pressure velocity, horizontal thermal advection, horizontal moisture advection, and the surface LH and SH fluxes in the large-scale forcing data for the two categories of events. For the model underestimation events, the large-scale meteorological backgrounds in the daytime and the nighttime are quite similar, with strong upward motions, weak horizontal thermal advection, and negative low-level horizontal moisture advection. For the model overestimation events, in the daytime there are weak vertical motions while in the nighttime there are moderate upward motions. There are strong positive low-level horizontal thermal advection and weak negative mid-to-high-level thermal advection, strong positive low-level horizontal moisture advection in both the daytime and nighttime with much stronger intensity in the nighttime. In the daytime there are very strong surface LH and SH fluxes, providing sufficient moisture supplies. The low-level warm and moist air convergence builds up a favorable condition for most SCMs (especially those CAPE-triggered-convection models) to produce strong convective precipitation especially in the daytime.

The results from this section highlight the dependence of model performance on large scale environments. The model underestimation events occur in the strong ascending regimes with negative low-level horizontal heat and moisture advection. The model overestimation events occur in the weak (in the daytime) or moderate (in the nighttime) ascending regimes with positive low-level horizontal heat and moisture advection. Moisture is supplied mainly by the surface evaporation in the day-time and by the positive horizontal moisture advection in the nighttime for model overestimation events.

5. Summary

This study quantitatively evaluates the statistical performances of the seven SCMs by comparing simulated precipitation with the observations from 1999 to 2001 at the ARM SGP site. The three-year long evaluation permits improved statistical evaluation of many aspects. It is found that although most SCMs can reproduce the observed total precipitation reasonably well, there are significant and interesting differences in their details, including differences between daytime and nighttime, between warm and cold seasons, between frequency and mean precipitation intensity, and between convective and stratiform partition. First, in the warm season, most SCMs produce more rain events in the daytime than in the nighttime while the observation has more rain events in the nighttime. The mean intensities of rain events in most SCMs are much stronger (weaker) in the daytime (nighttime) than the observation. In the cold season, the model-observation differences in the frequency and mean intensity of rain events tend to compensate each other for most SCMs. In the daytime, most SCMs have higher frequency of moderate-to-strong precipitation events (10 mm/day to 50 mm/day) than the observation in the warm season. In the nighttime, all the SCMs have lower frequency of moderate-to-strong precipitation events (>10 mm/day) than the observation for both warm and cold seasons. Second, the higher frequency of warm season daytime precipitation events in most SCMs is related to the fact that most SCMs produce a spurious precipitation peak around the regime of weak vertical motions. The spurious precipitation peak is mainly produced by the strong convective precipitation when precipitable water and relative humidity are large. Third, analyses of extreme events reveal distinct meteorological backgrounds for model underestimation and overestimation events. The model underestimation events occur in the strong ascending regimes with negative low-level horizontal heat and moisture advection whereas model overestimation events occur in the weak (in the daytime) or moderate (in the nighttime) ascending regimes with positive low-level horizontal heat and moisture advection. Moisture is supplied mainly by the surface evaporation

in the day-time and by the positive horizontal moisture advection in the nighttime for model overestimation events.

The different SCM performances and associations with large scale forcing and thermodynamic factors also shed useful insights on convection parameterizations and future development. For example, the analysis also reveals that the convective precipitation is much weaker in the GISS SCM (Figures 5 and 7). According to Del Genio and Wolf (2012), this may be related to the parcel-lifting-based trigger used in the convection scheme. The GISS SCM often cannot convect under the observed thermodynamic structure at the time the observed precipitation begins because the turbulent kinetic energy (TKE) is not strong enough to provide updrafts to lift the air parcel to the level of free convection against large CIN within one time step. On the other hand, the models using CAPE-based triggers can produce convective precipitation even under the condition with large CIN. However, there is no observational support for such CAPE-based triggers (Jakob 2011). Moreover, the relevant forcing for many convective situations at the SGP site is mesoscale in nature and is thus absent or inaccurately represented in both the forcing and the parameterizations themselves. Whether the SCM with today's cumulus parameterizations, which are forced with the large-scale information and parameterize only cloud-scale response to that forcing, should convect at the SGP site is still an open question. More investigation is in order along this line.

Acknowledgement: This work is part of the FASTER project (http://www.bnl.gov/esm/) supported by DOE Earth System Model program.

Reference

Ackerman, T. P., and G. M. Stokes, 2003: The Atmospheric Radiation Measurement Program, *Physics Today*, 39-44.

Bechtold, P., and Coauthors, 2004: The simulation of the diurnal cycle of convective precipitation over land in a global model, *Q. J. R. Meteorol. Soc*., *130*, 3119-3137.

Betts, A. K., and C. Jakob, 2002: Study of diurnal cycle of convective precipitation over Amazonia using a single column model, *J. Geophys. Res*., *107*(D23), 4732, doi:10.1029/2002JD002264.

Bretherton, C. S., M. E. Peters, and L. E. Back, 2004: Relationships between water vapor path and precipitation over the tropical oceans, *J. Climate*, *17*, 1517-1528.

Dai, A., and K. E. Trenberth, 2004: The diurnal cycle and its depiction in the Community Climate System Model, *J. Climate*, *17*, 930-951.

——, 2006: Precipitation characteristics in eighteen coupled climate models, *J. Climate*, *19*, 4605-4630.

Del Genio, A. D., and M. Yao, 1993: Efficient cumulus parameterization for long-term climate studies: The GISS scheme, in *The Representation of Cumulus Convection in Numerical Models*, AMS Meteor. Monograph., K.A. Emanuel and D.A. Raymond, Eds., vol. *24*, 46. *American Meteorological Society*, pp. 181-184.

——, A. D., M.-S. Yao, W. Kovari, and K.K.-W. Lo, 1996: A prognostic cloud water parameterization for global climate models, *J. Climate*, *9*, 270–304.

——, W. Kovari, M.-S. Yao, and J. Jonas, 2005: Cumulus microphysics and climate sensitivity, *J. Climate*, *18*, 2376-2387, doi:10.1175/JCLI3413.1.

——, M.-S. Yao, and J. Jonas, 2007: Will moist convection be stronger in a warmer climate? *Geophys. Res. Lett.*, *34*, L16703, doi:10.1029/2007GL030525.

——, and A. Wolf, 2012: Should today's SCMs convect at the SGP? *FASTER Breakout, ASR Science Team Meeting,* March 12, 2012.

Donner, L. J., C. J. Seman, R. S. Hemiler, and S. Fan, 2001: A cumulus parameterization including mass fluxes, convective vertical velocities, and mesoscale effects: Thermodynamic and hydrological aspects in a general circulation model, *J. Climate*, *14*, 3444–3463.

——, and Coauthors, 2011: The dynamical core, physical parameterizations, and basic simulation characteristics of the atmospheric component AM3 of the GFDL global coupled model CM3. *J. Climate*, **24**, 3484–3519.

Ghan, S. J., X. Bian, and L. Corsetti, 1996: Simulation of the Great Plains low-level jet and associated clouds by general circulation models, *Mon. Weather Rev., 124*, 1388–1408.

——, and Coauthors, 2000: An intercomparison of single column model simulations of summertime midlatitude continential convection, *J. Geophys. Res*., *105*, 2091-2124.

Gregory, D., Morcrette, J.-J., Jakob, C., Beljaars, A. M. and Stockdale, T., 2000: Revision of convection, radiation and cloud schemes in the ECMWF Integrated Forecasting System. *Q. J. R. Meteorol. Soc.*, 126, 1686–1710.

Hack, J. J., 1994: Parameterization of moist convection in the National Center for Atmospheric Research Center Community Climate Model (CCM2). *J. Geophys. Res., 99*, 5551-5568.

——, J. A. Pedretti, 2000: Assessment of solution uncertainties in Single-Column Modeling frameworks. *J. Climate*, 13, 352–365.

Jakob, C., L. Davies, V. Kumar, and P. May, 2011: Representing convection in models – How stochastic does it need to be? *Proceeding of the ECMWF Workshop on "Representing Model Uncertainty and Error in Weather and Climate Prediction",* ECMWF, June 2011.

Kennedy, A. D., and Coauthors, 2010: Evaluation of the NASA GISS Single Column Model simulated clouds using combined surface and satellite observations, *J. Climate, 23*, 5175-5192.

Lee, M-I, and Coauthors, 2007: An analysis of the warm-season diurnal cycle over the continental United States and northern Mexico in general circulation models, *J. Hydrometeor.*, *8*, 344-366.

——, and S. D. Schubert, 2008: Validation of the diurnal cycle in the NASA's modern era retrospective-analysis for research and applications (MERRA), In: Proceedings of the 88th AMS annual meeting, 20–24 January, New Orleans.

——, and Coauthors, 2008: Role of convection triggers in the simulation of the diurnal cycle of precipitation over the United States Great Plains in a general circulation model, *J. Geophys. Res*., *113*, D02111, doi: 10.1029/2007JD008984.

Lin, J.-L., 2007: The double-ITCZ problem in IPCC AR4 coupled GCMs: Ocean–atmosphere feedback analysis, *J. Climate*, *20*, 4497–4525.

Moorthi, S., and M. J. Suarez, 1992: Relaxed Arakawa-Schubert: A parameterization of moist convection for general circulation models, *Mon. Weather Rev*., *120*, 978-1002.

Morrison, H., and A. Gettelman, 2008: A new two-moment bulk stratiform cloud microphysics scheme in the Community Atmospheric Model (CAM3), Part I: Description and numerical tests, *J. Climate*, *21*, 3845-3862.

Neale, R. B., J. H. Richter, and M. Jochum, 2008: The impact of convection on ENSO: from a delayed oscillator to a series of events, *J. Climate*, *21*, 5904-5924.

Neggers, R. A. J., A. P. Siebesma, and T. Heus, 2012: Continuous single-column model evaluation at a permanent meteorological supersite, *Bull. Amer. Meteor. Soc.*, *in press.*

Park, S., and C. S. Bretherton, 2009: The University of Washington shallow convection and moist turbulence schemes and their impact on climate simulations with the community atmosphere model, *J. Climate., 22*, 3449-3469.

——, C. S. Bretherton, and P. J. Rasch, 2010: The revised cloud macrophysics in the community atmosphere model, *J. Climate*, *in preparation*.

Randall, D., and D. G. Cripe, 1999: Alternative methods for specification of observed forcing in single-column models and cloud system models, *J. Geophys. Res*., *104*(D20), 24,527–24,545, doi:10.1029/1999JD900765.

——, and Coauthors, 2003: Confronting models with data: The GEWEX Cloud Systems Study, *Bull. Amer. Meteorol. Soc., 84*, 455-469.

Rasch, P. J., and J. E. Kristjansson, 1998: A comparison of the CCM3 model climate using diagnosed and predicted condensate parameterizations, *J. Climate*, *11*, 1587-1614.

Rotstayn, L. D., 1997: A physical based scheme for the treatment of stratiform clouds and precipitation in large-scale models. I: Description and evaluation of the microphysical processes, *Q. J. R. Meteorol. Soc*., *123*, 1227-1282.

Salzmann, M., and Coauthors, 2010: Two-moment bulk stratiform cloud microphysics in the GFDL AM3 GCM: description, evaluation, and sensitivity tests, *Atmos. Chem. Phys*., *10*, 8037–8064, doi:10.5194/acp-10-8037-2010.

Schmidt, G.A., and Coauthors, 2006: Present day atmospheric simulations using GISS ModelE: Comparison to in-situ, satellite and reanalysis data. *J. Climate*, 19, 153-192.

——, and Coauthors, 2012: Configuration and assessment of the GISS Model E2 contributions to the CMIP5 archive, *in preparation.*

Stokes, G. M., and S. E. Schwartz, 1994: The Atmospheric Radiation Measurement (ARM) Program: Programmatic Background and Design of the Cloud and Radiation Testbed, *Bull. Amer. Meteor. Soc.*, *75*, 1201 – 1221.

Sun, Y., S. Solomon, A. Dai, and R. W. Portmann, 2006: How often does it rain?, *J. Climate*, *19*, 916–934.

Tiedtke, M., 1989: A comprehensive mass flux scheme for cumulus parameterization in large-scale models, *Mon. Wea. Rev*., *117*, 1779-1800.

——, 1993: Representation of clouds in large-scale models, *Mon. Weather Rev*., *121*, 3040-3061.

Xie, S., and M. Zhang, 2000: Impact of the convection trigger function on single-column model simulations, *J. Geophys. Res., 105*(D11), 14983-14996, doi: 10.1029/2000JD900170.

——, and Coauthors, 2002: Intercomparison and evaluation of cumulus parameterizations under summertime midlatitude continental conditions, *Q. J. R. Meteorol. Soc.*, *128*, 1095-1135.

——, R. T. Cederwall, and M. Zhang, 2004: Developing long-term single-column model/cloud system-resolving model forcing data using numerical weather prediction products constrained by surface and top of atmosphere observations, *J. Geophys. Res*., *109*, D01104, doi: 10.1029/2003JD004045.

——, and Coauthors, 2005: Simulations of midlatitude frontal clouds by single-column and cloud-resolving models during the Atmospheric Radiation Measurement March 2000 cloud intensive operational period, *J. Geophys. Res*., *110*, D15S03, doi: 10.1029/2004JD005119.

Zhang, G. J., and N. A. McFarlane, 1995: Sensitivity of climate simulations to the parameterization of cumulus convection in the Canadian Climate Center general circulation model, *Atmos. Ocean*, *33*, 407-446.

——, 2003: Roles of tropospheric and boundary layer forcing in the diurnal cycle of convection in the US Southern Great Plains, *Geophys. Res. Lett*., *30*, doi: 10.1029/2003GL018554.

Zhao, M., W. Lin, C. S. Bretherton, J. J. Hack, and P. J. Rasch, 2003: A modified formulation of fractional stratiform condensation rate in the NCAR community atmospheric model CAM2, *J. Geophys. Res*., 108 (D1), 4035, doi:10.1029/2002JD002523.

——, I.M. Held, S-J. Lin, and G.A. Vecchi, 2009: Simulations of global hurricane climatology, interannual variability, and response to global warming using a 50km resolution GCM. *J. Climate*, 33, 6653-6678.

Table List

Table 1. Summary of Participating SCMs and Main Related Parameterizations.

Figure List

Figure 1: Frequency of specified model biases in total precipitation for all-time (solid lines), daytime (dash lines in upper panel) and nighttime (dash dotted lines in lower panel) data.

Figure 2: Same as Figure 1 but for warm season (left panel) and cold season (right panel) respectively.

Figure 3: Frequency (left-y) and mean intensity (right-y) of rain events (Pr>0.1mm/day) for all season (a), warm season (b) and cold season (c) respectively. Units of frequency and intensity are % and mm/day respectively.

Figure 4: Frequency of daytime total precipitation for warm season (a) and cold season (b) respectively. Frequency of nighttime total precipitation for warm season (c) and cold season (d) respectively. Unit of frequency is %.

Figure 5: Ratios of convective precipitation to total precipitation in daytime for warm season (a) and cold season (b), and in nighttime for warm season (c) and cold season (d) respectively. Unit of ratio is %.

Figure 6: Scatter-plots of 500hPa vertical pressure velocity (w500) and total precipitation for precipitation events only (Pr>0.1mm/day) in ARM observation and 7 SCMs for daytime (red dots) and nighttime (blue dots) respectively. Units of w500 and precipitation are hPa/day and mm/day respectively.

Figure 7: Averaged total precipitation, stratiform precipitation and convective precipitation binned by PW daytime (left panel) and nighttime (right panel) precipitation events (Pr>0.1mm/day) respectively. Unit of precipitation is mm/day.

Figure 8: Joint probability density function (shaded) and averaged total precipitation (contours) binned by w500 and PW for precipitation events only (Pr>0.1mm/day) in ARM observation and 7 SCMs. Units of w500, PW, PDF and precipitation are hPa/day, mm, % and mm/day respectively.

Figure 9: Averaged total precipitation (shaded) and joint PDF of relative humidity (RH) (contours) binned by RH and PW for precipitation events only (Pr>0.1mm/day) in ARM observation and 7 SCMs when |w500|<50hPa/day. Units of RH, PW, precipitation and PDF are %, mm, mm/day and % respectively.

Figure 10: Same as Figure 9 except for convective precipitation in 7 SCMs and total precipitation in ARM observation.

Figure 11: Averaged total precipitation amounts in 7 SCMs and ARM observation for events with dPr<-20mm/day for all the SCMs, dPr>10mm/day for certain SCMs in the daytime (D) and nighttime (N) respectively. Total precipitation difference (dPr) is defined as: Pr in SCM minus Pr in Obs. Asteroids represent the averaged convective precipitation amounts in 7 SCMs.

Figure 12: Vertical profiles of averaged vertical pressure velocity (a), horizontal T advection (b), horizontal q advection (c), and averaged surface fluxes (d) in the large-scale continuous forcing data for events with dPr<-20mm/day for all the SCMs, dPr>10mm/day for certain SCMs in the daytime (D) and nighttime (N) respectively. Units of vertical pressure velocity, horizontal T advection, horizontal q advection and surface fluxes are hPa/day, K/day, g/kg/day and W/m^2, respectively.

Table 1. Summary of Participating SCMs and Main Related Parameterizations

Models	Convection Scheme	Cloud Scheme	Resolution
GFDL AM2	Relaxed AS (deep and shallow) Moorthi and Suarez 1992	1-moment Microphysics Rotstayn 1997 Cloud Macrophysics Tiedtke 1993	L24, 30mn
GFDL AM3*	Donner (deep) Donner et al. 2001; Donner et al. 2011 UW (shallow) Zhao et al. 2009	1-moment Microphysics Rotstayn 1997 Cloud Macrophysics Tiedtke 1993	L24, 30mn
GISS Model E2+	Bulk mass flux (deep and shallow) Del Genio and Yao 1993; Del Genio et al. 2007 Del Genio et al. 2005 (Cumulus microphysics)	Micro/Macro-physics Del Genio et al. 1996 Schmidt et al. 2006 Schmidt et al. 2012	L40, 30mn
ECMWF IFS	Bulk mass flux (deep and shallow) Tiedtke 1989 Gregory et al. 2000	1-moment Microphysics Tiedtke 1993; Gregory et al. 2000 Cloud Macrophysics Tiedtke 1993; Gregory et al. 2000	L91, 5mn
NCAR CAM3	Simplified AS (deep) Zhang and McFarlane 1995 Hack (shallow) Hack 1994	1-moment Microphysics Rasch and Kristjansson 1998 Cloud Macrophysics Zhang et al. 2003	L26, 20mn
NCAR CAM4	Modified ZM (deep) Neale et al. 2008 Hack (shallow) Hack 1994	1-moment Microphysics Rasch and Kristjansson 1998 Cloud Macrophysics Zhang et al. 2003	L26, 20mn
NCAR CAM5	Modified ZM (deep) Neale et al. 2008 UW (shallow) Park and Bretherton 2009	2-moment Microphysics Morrison and Gettelman 2008 Cloud Macrophysics Park et al. 2010	L30, 20mn

AS is Arakawa and Schubert (1974)

ZM is Zhang and McFarlane (1995)

* The implementation of the deep cumulus parameterization in GFDL AM3 differs from Donner et al. (2001), as described in Donner et al. (2011). Also, the single-column version of AM3 differs from the GCM described in Donner et al. (2011) by using a specified droplet concentration of 300 cm^{-3} instead of interactive aerosols and chemistry.

+ The single-column version of GISS Model E2 in this study uses 1-moment cloud microphysics scheme, while the full GISS Model E2 uses 2-moment microphysics scheme.

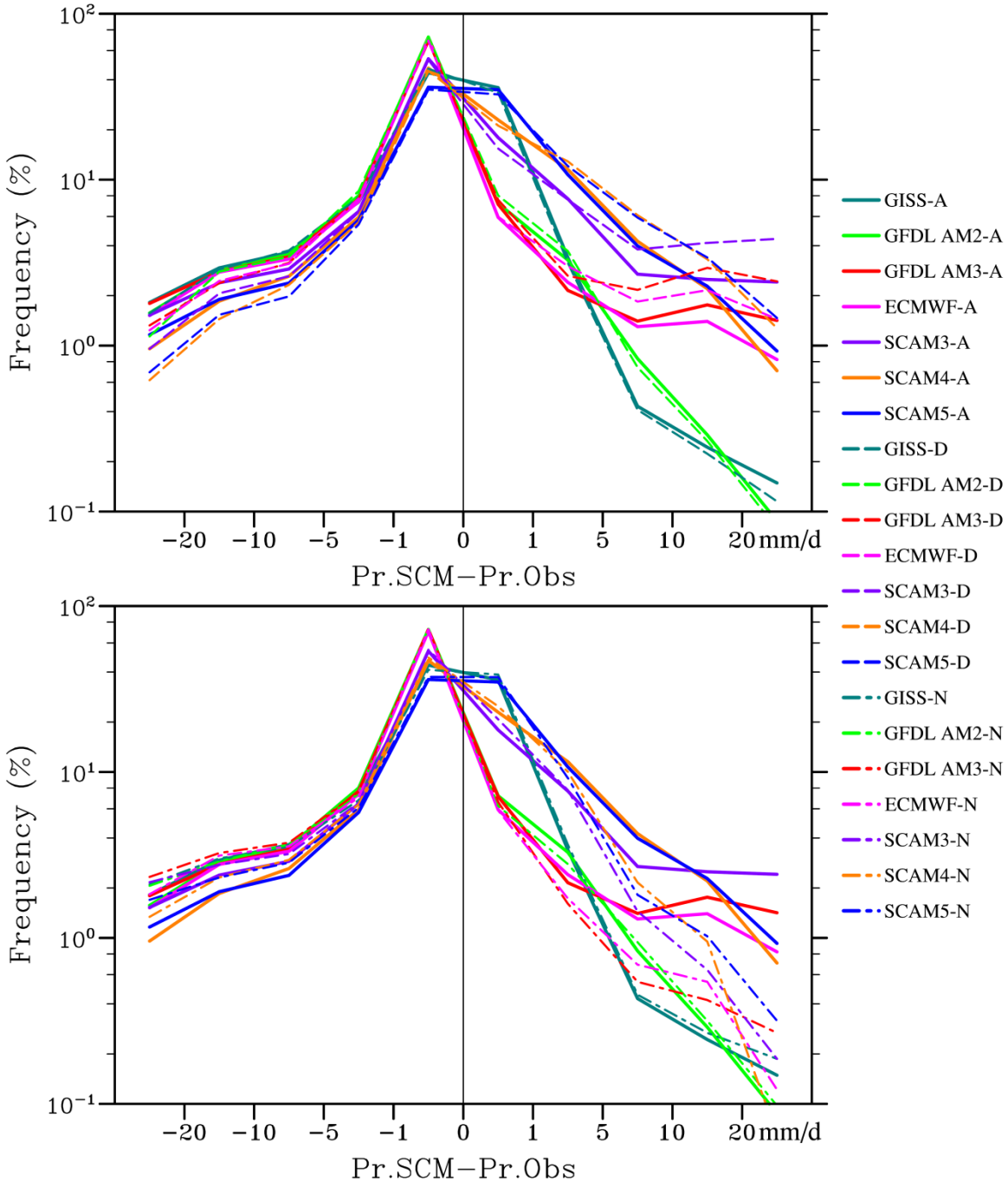

Figure 1: Frequency of specified model biases in total precipitation for all-time (solid lines), daytime (dash lines in upper panel) and nighttime (dash dotted lines in lower panel) data.

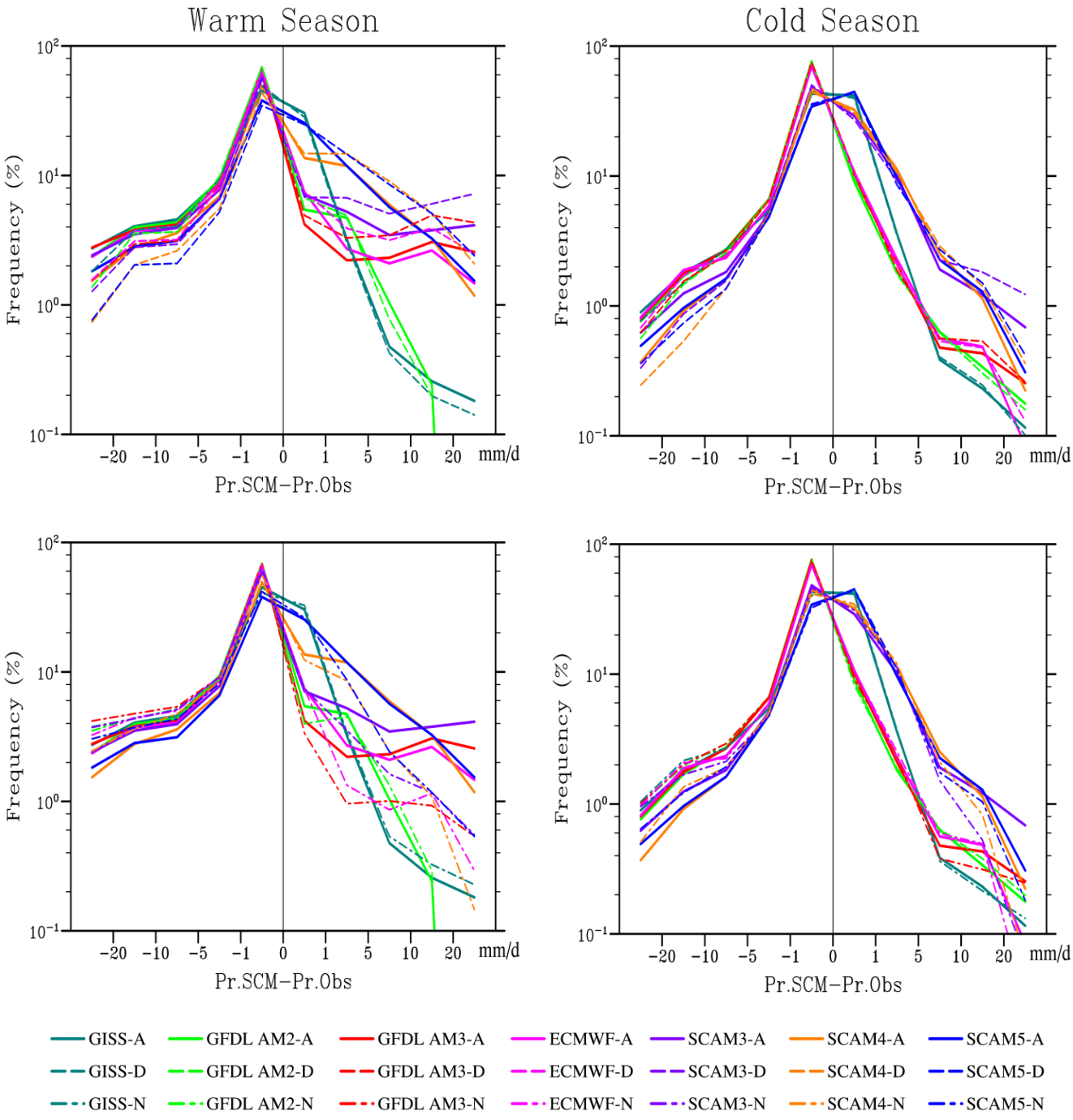

Figure 2: Same as Figure 1 but for warm season (left panel) and cold season (right panel) respectively.

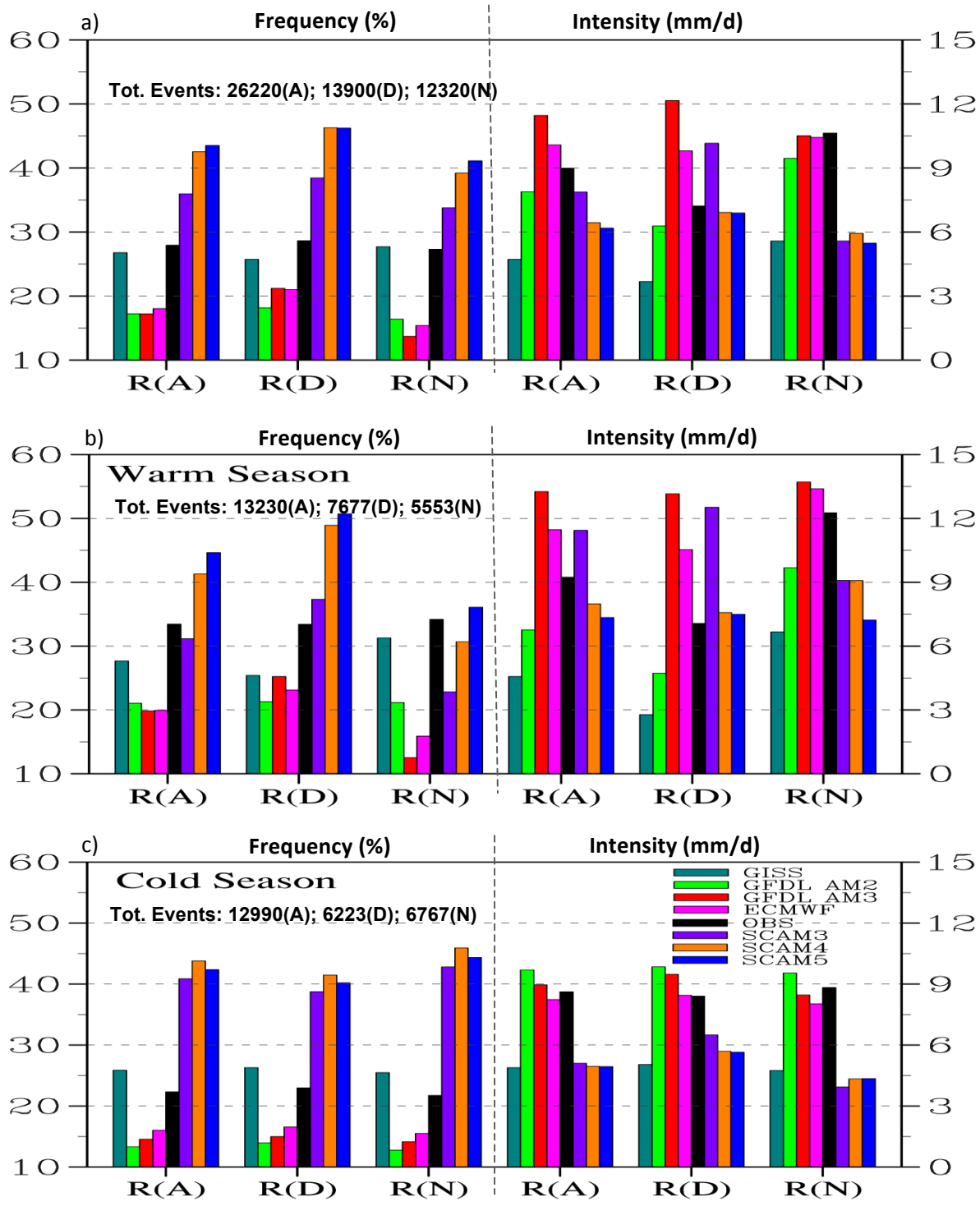

Figure 3: Frequency (left-y) and mean intensity (right-y) of rain events (Pr>0.1mm/day) for all season (a), warm season (b) and cold season (c) respectively. Units of frequency and intensity are % and mm/day respectively.

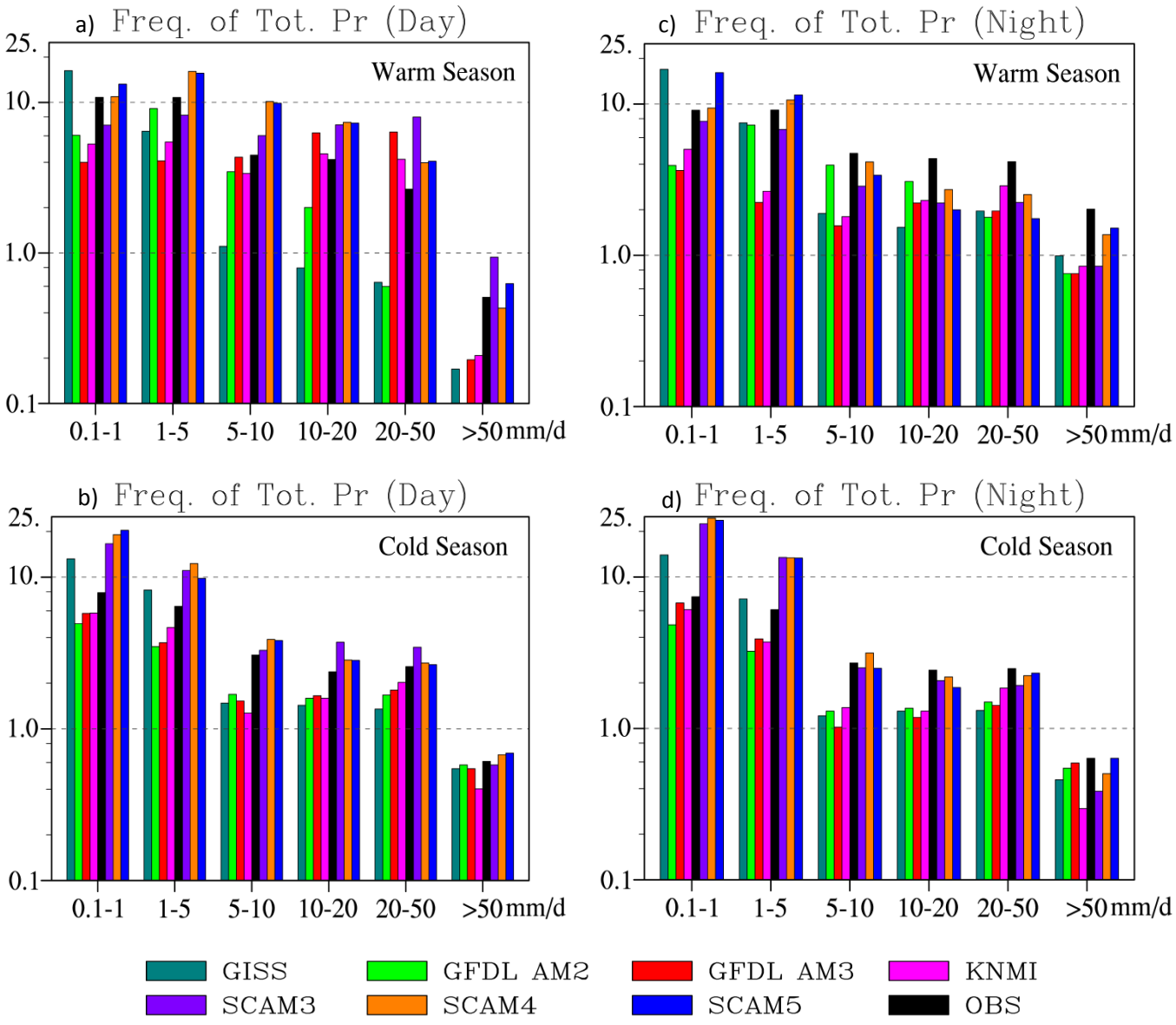

Figure 4: Frequency of daytime total precipitation for warm season (a) and cold season (b) respectively. Frequency of nighttime total precipitation for warm season (c) and cold season (d) respectively. Unit of frequency is %.

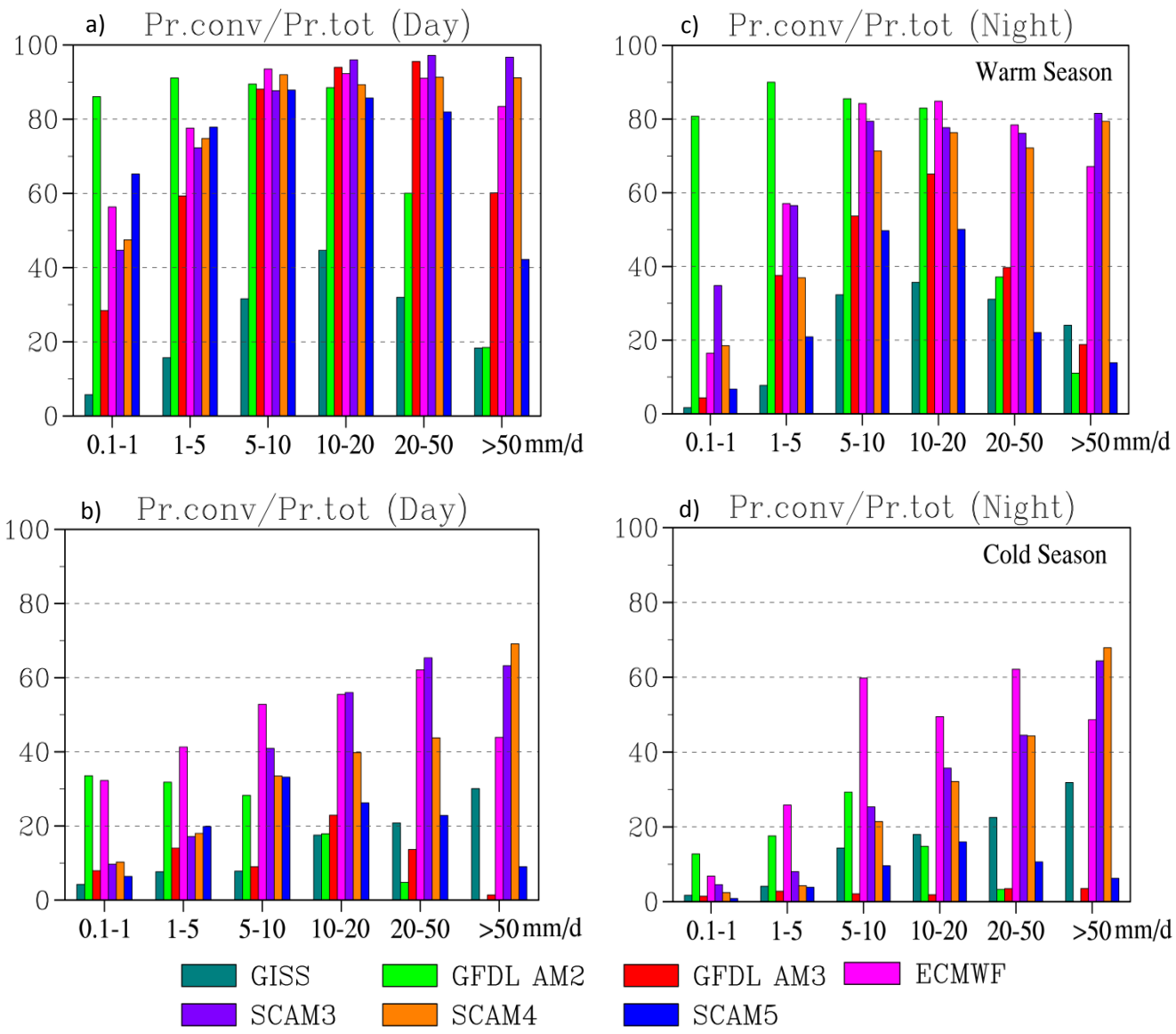

Figure 5: Ratios of convective precipitation to total precipitation in daytime for warm season (a) and cold season (b), and in nighttime for warm season (c) and cold season (d) respectively. Unit of ratio is %.

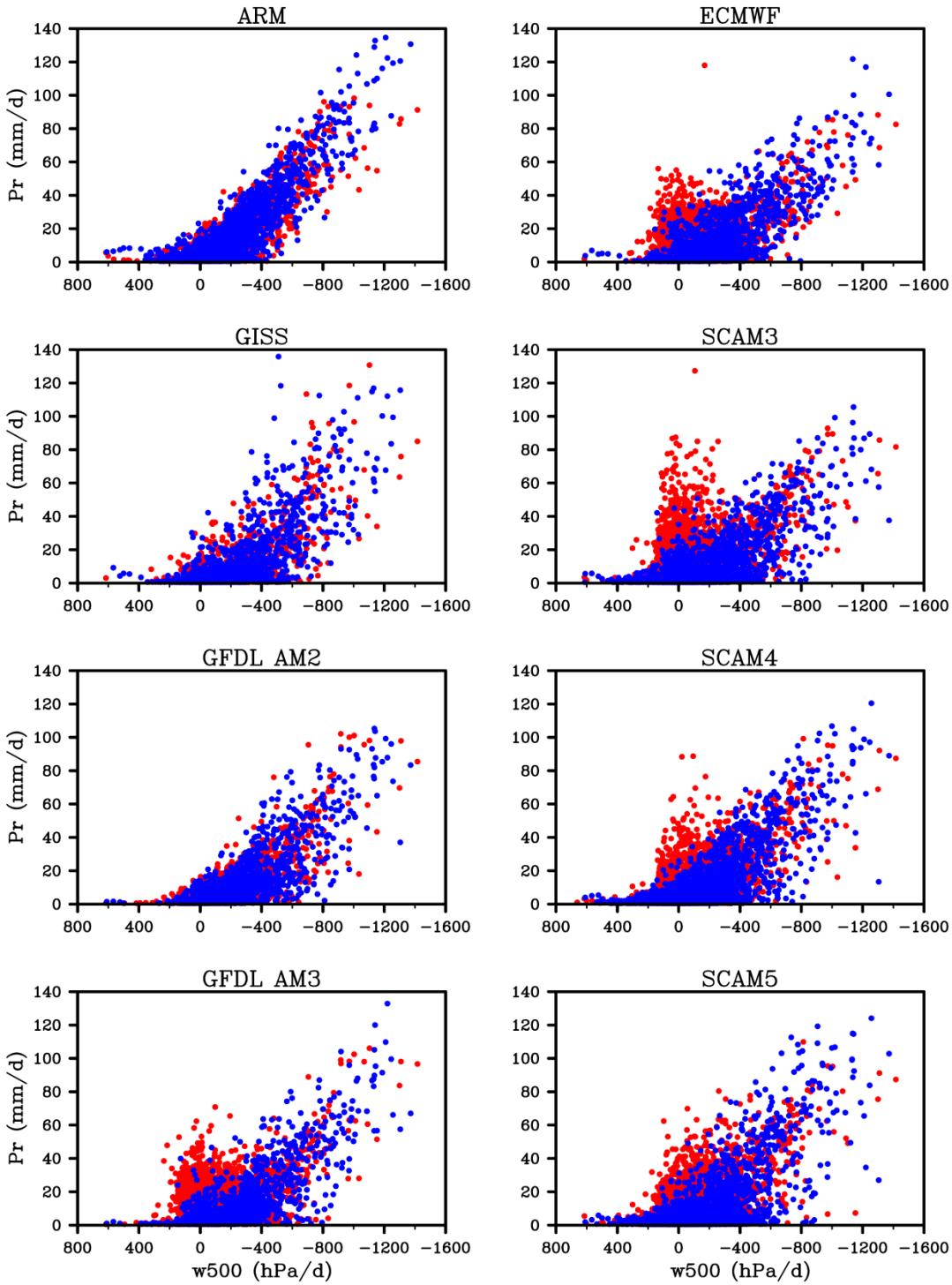

Figure 6: Scatter-plots of 500hPa vertical pressure velocity (w500) and total precipitation for precipitation events only (Pr>0.1mm/day) in ARM observation and 7 SCMs for daytime (red dots) and nighttime (blue dots) respectively. Units of w500 and precipitation are hPa/day and mm/day respectively.

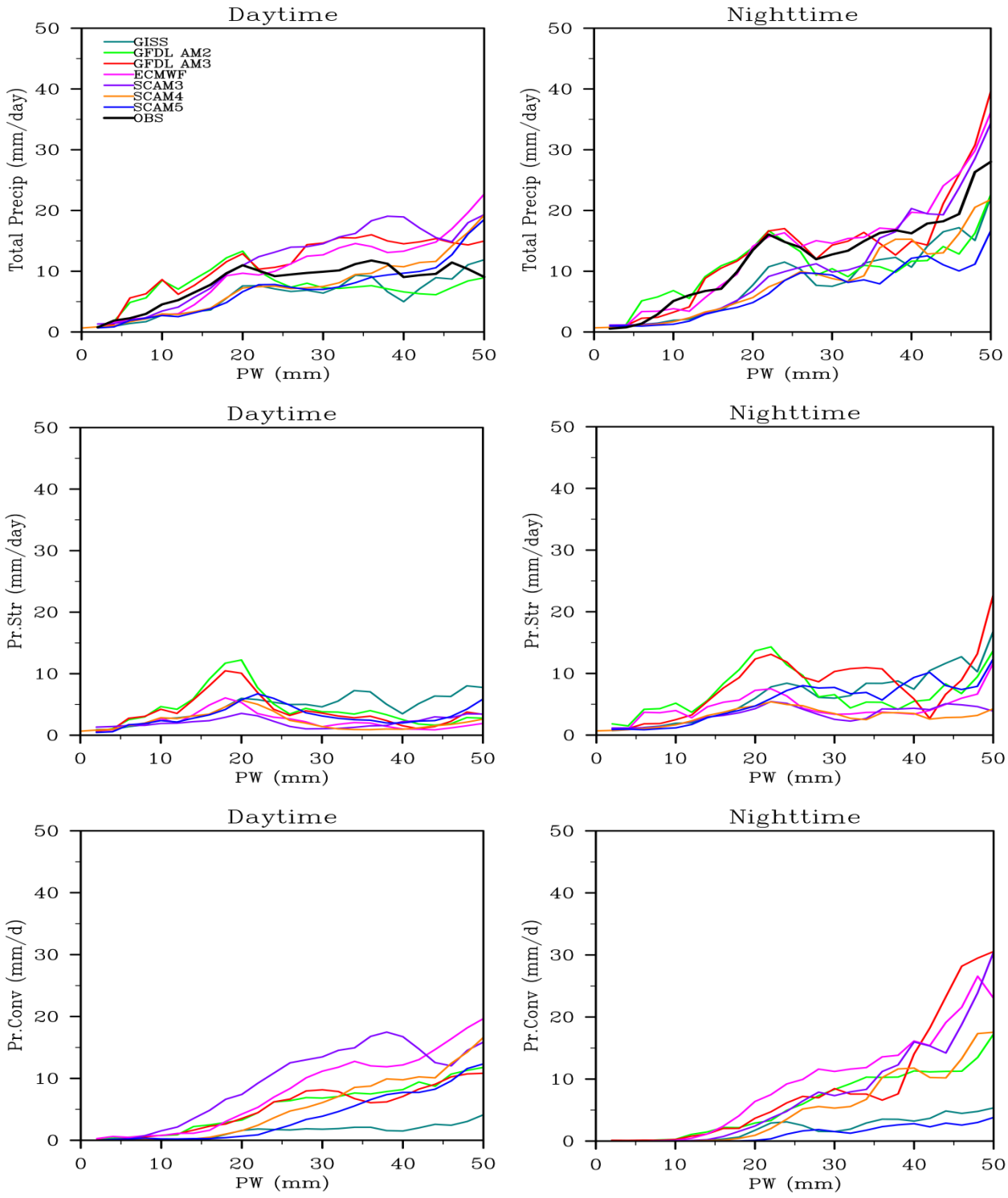

Figure 7: Averaged total precipitation, stratiform precipitation and convective precipitation binned by PW daytime (left panel) and nighttime (right panel) precipitation events (Pr>0.1mm/day) respectively. Unit of precipitation is mm/day.

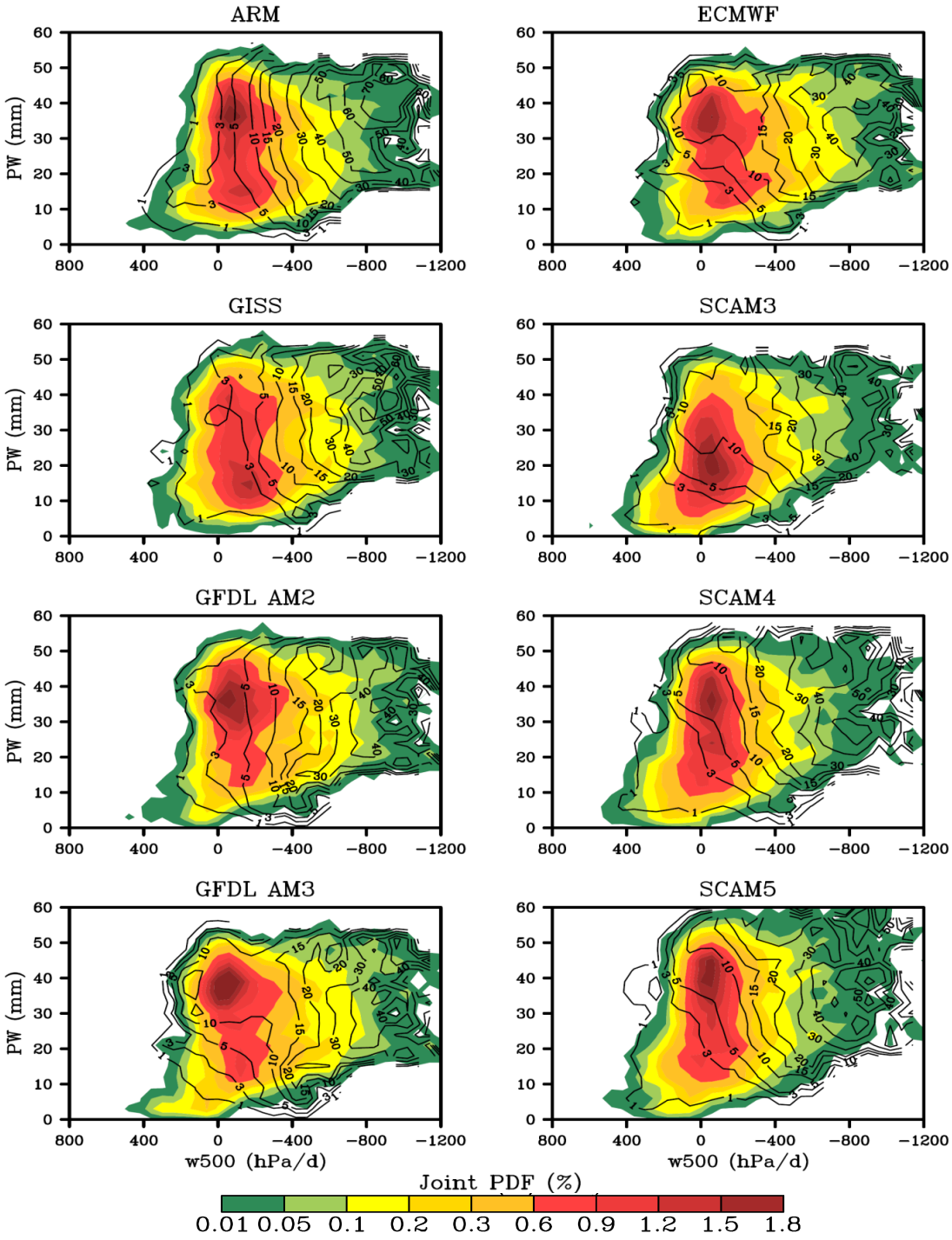

Figure 8: Joint probability density function (shaded) and averaged total precipitation (contours) binned by w500 and PW for precipitation events only (Pr>0.1mm/day) in ARM observation and 7 SCMs. Units of w500, PW, PDF and precipitation are hPa/day, mm, % and mm/day respectively.

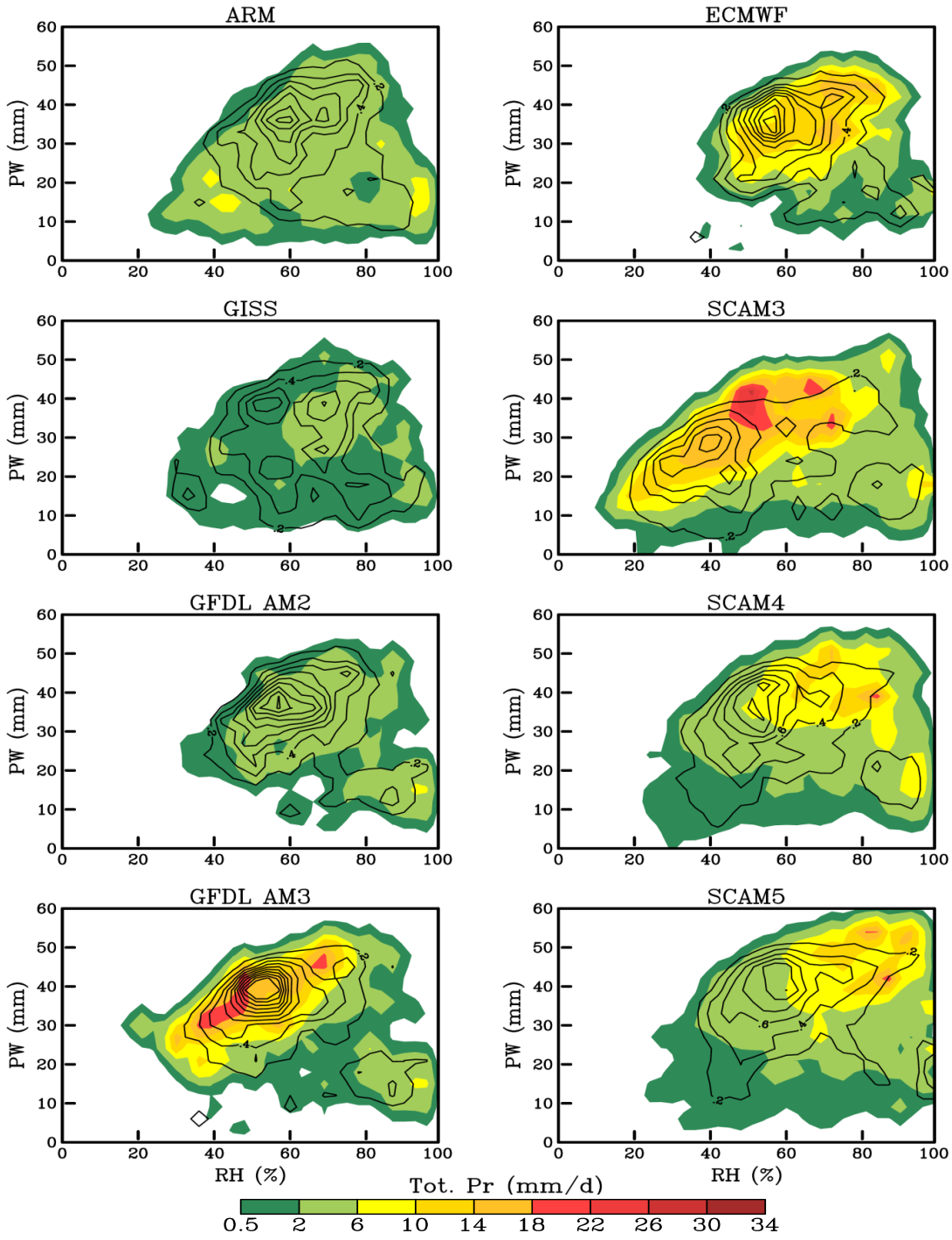

Figure 9: Averaged total precipitation (shaded) and joint PDF of relative humidity (RH) (contours) binned by RH and PW for precipitation events only (Pr>0.1mm/day) in ARM observation and 7 SCMs when |w500|<50hPa/day. Units of RH, PW, precipitation and PDF are %, mm, mm/day and % respectively.

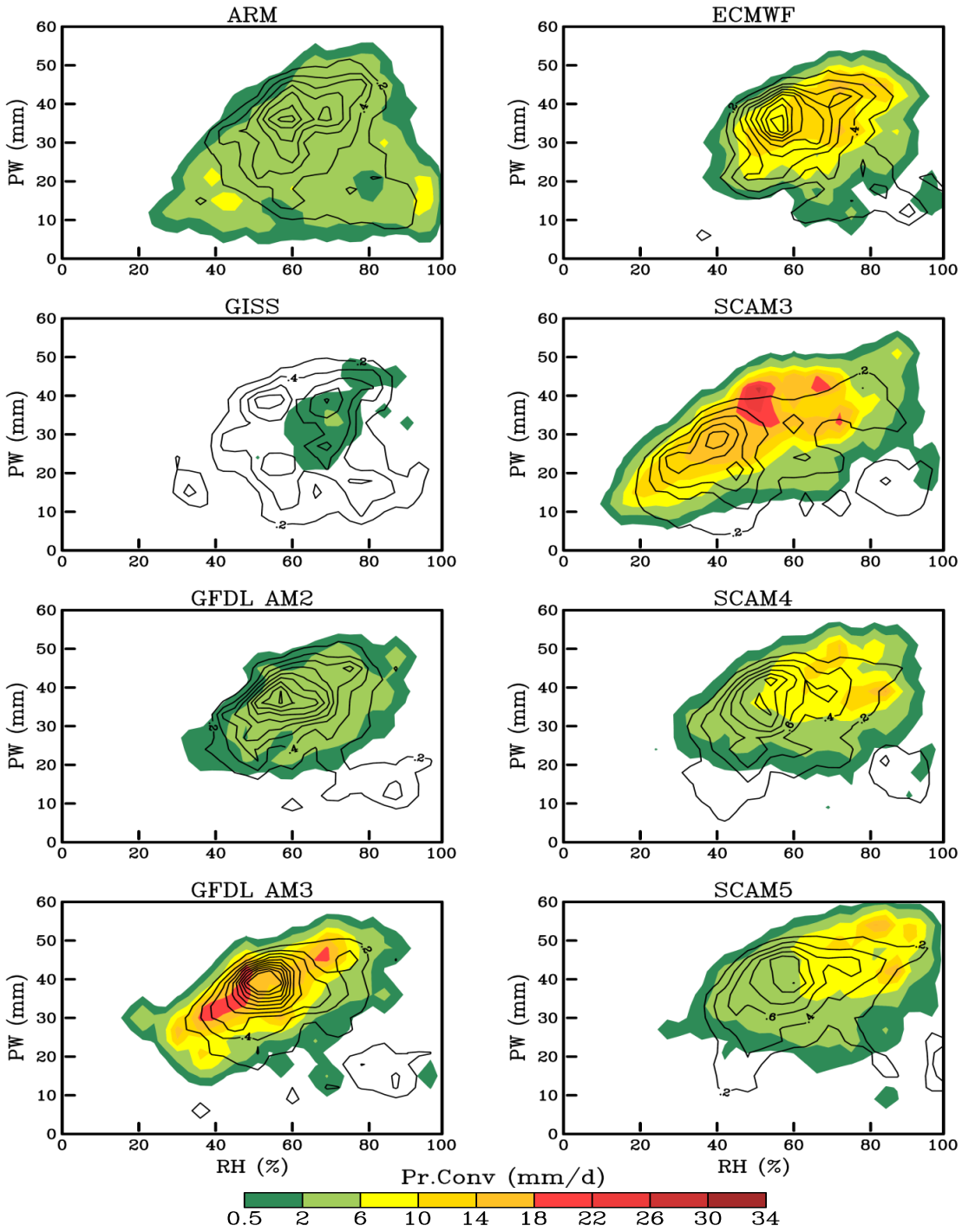

Figure 10: Same as Figure 9 except for convective precipitation in 7 SCMs and total precipitation in ARM observation.

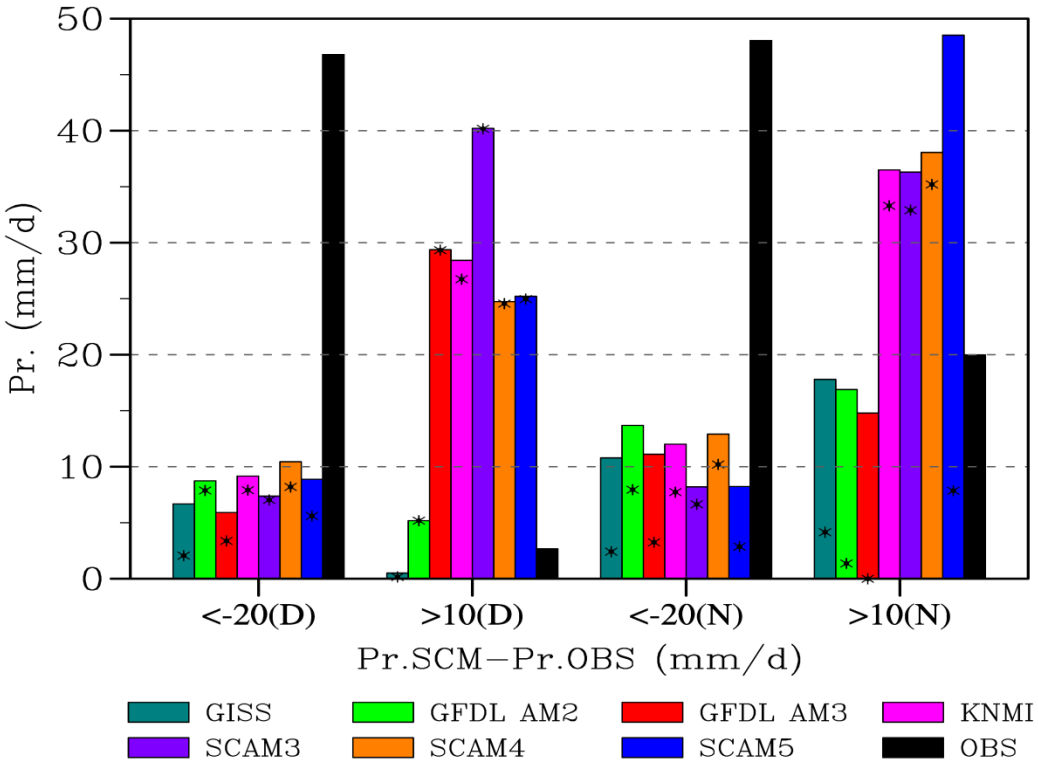

Figure 11: Averaged total precipitation amounts in 7 SCMs and ARM observation for events with dPr<-20mm/day for all the SCMs, dPr>10mm/day for certain SCMs in the daytime (D) and nighttime (N) respectively. Total precipitation difference (dPr) is defined as: Pr in SCM minus Pr in Obs. Asteroids represent the averaged convective precipitation amounts in 7 SCMs.

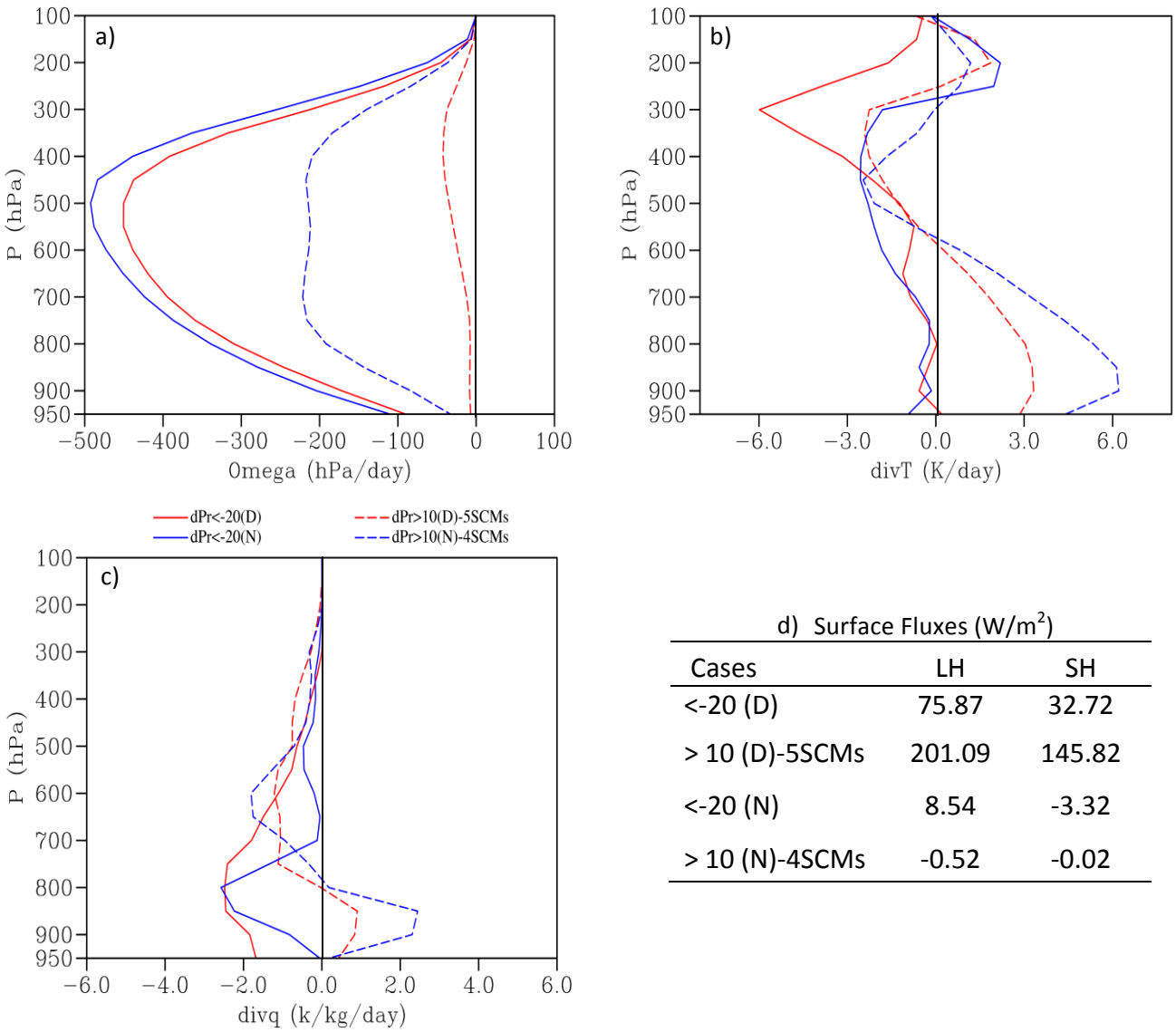

d) Surface Fluxes (W/m^2)

Cases	LH	SH
<-20 (D)	75.87	32.72
> 10 (D)-5SCMs	201.09	145.82
<-20 (N)	8.54	-3.32
> 10 (N)-4SCMs	-0.52	-0.02

Figure 12: Vertical profiles of averaged vertical pressure velocity (a), horizontal T advection (b), horizontal q advection (c), and averaged surface fluxes (d) in the large-scale continuous forcing data for events with dPr<-20mm/day for all the SCMs, dPr>10mm/day for certain SCMs in the daytime (D) and nighttime (N) respectively. Units of vertical pressure velocity, horizontal T advection, horizontal q advection and surface fluxes are hPa/day, K/day, g/kg/day and W/m^2, respectively.

Supplementary Figure List

Figure S1: Same as in Figure 6 except for warm season.

Figure S2: Same as in Figure 6 except for cold season.

Figure S3: Same as in Figure 8 except for warm season.

Figure S4: Same as in Figure 8 except for cold season.

Figure S5: Same as in Figure 8 except for daytime.

Figure S7: Same as in Figure 10 except for daytime.

Figure S8: Same as in Figure 10 except for nighttime.

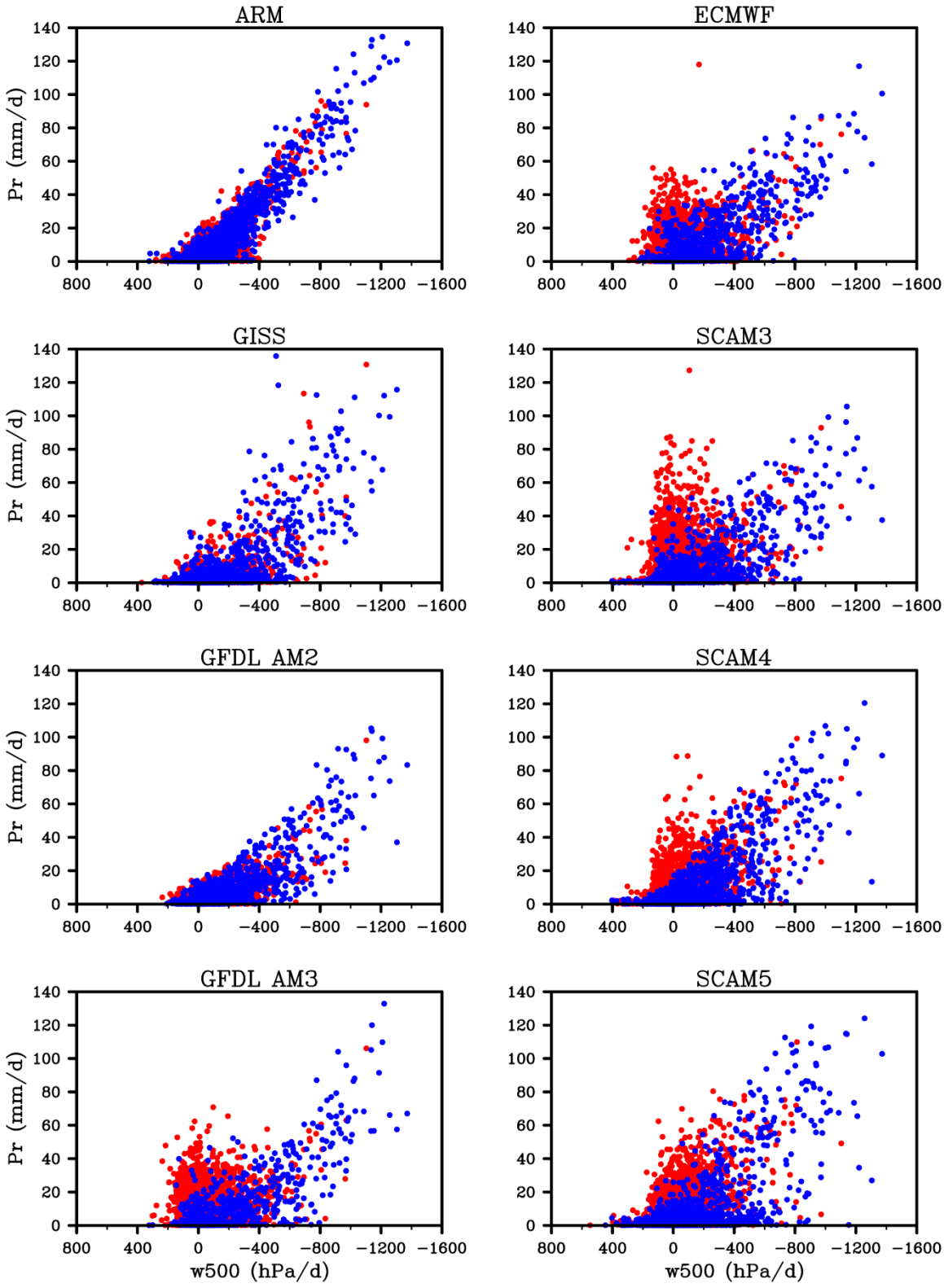

Figure S1: Same as in Figure 6 except for warm season.

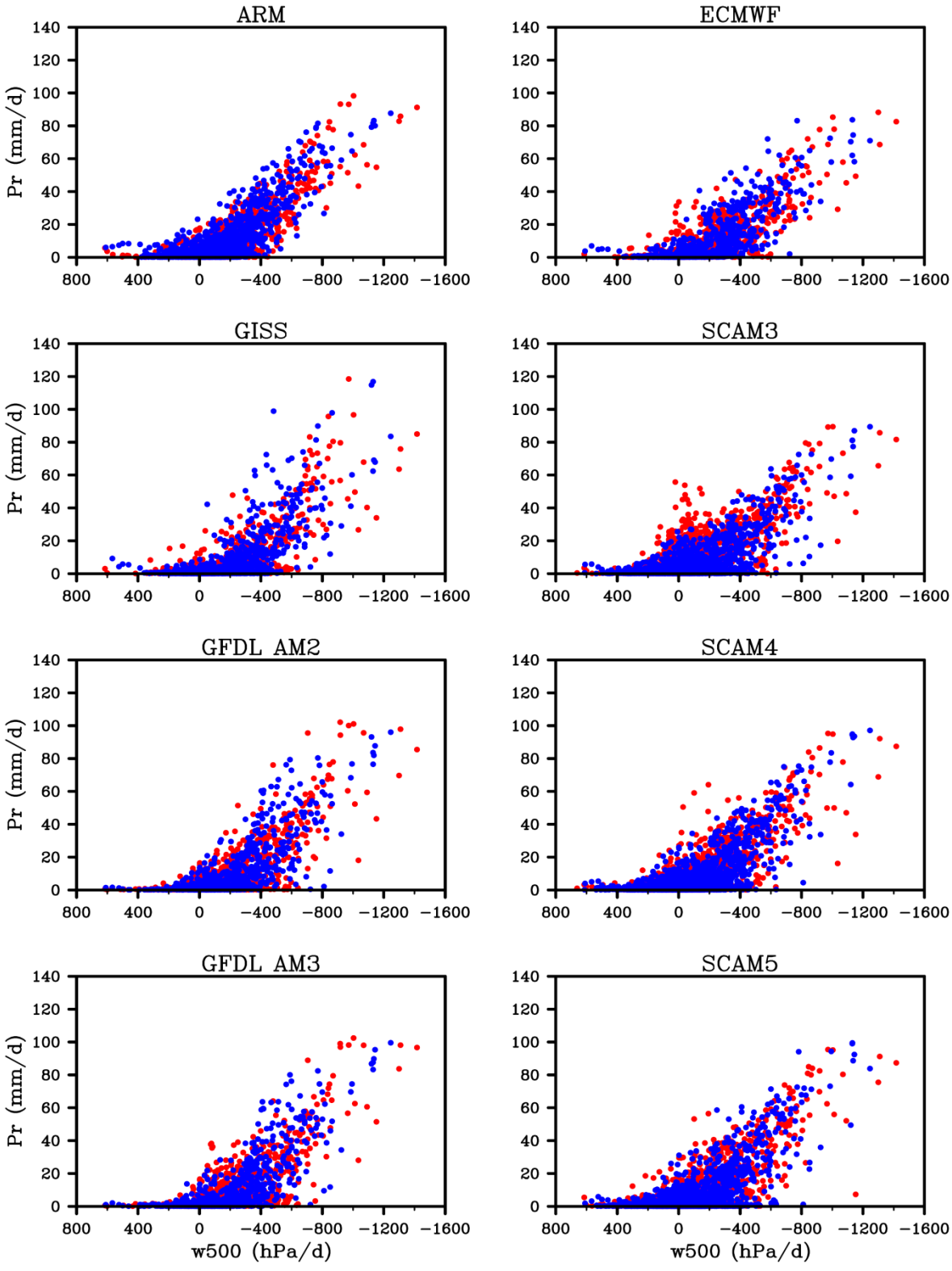

Figure S2: Same as in Figure 6 except for cold season.

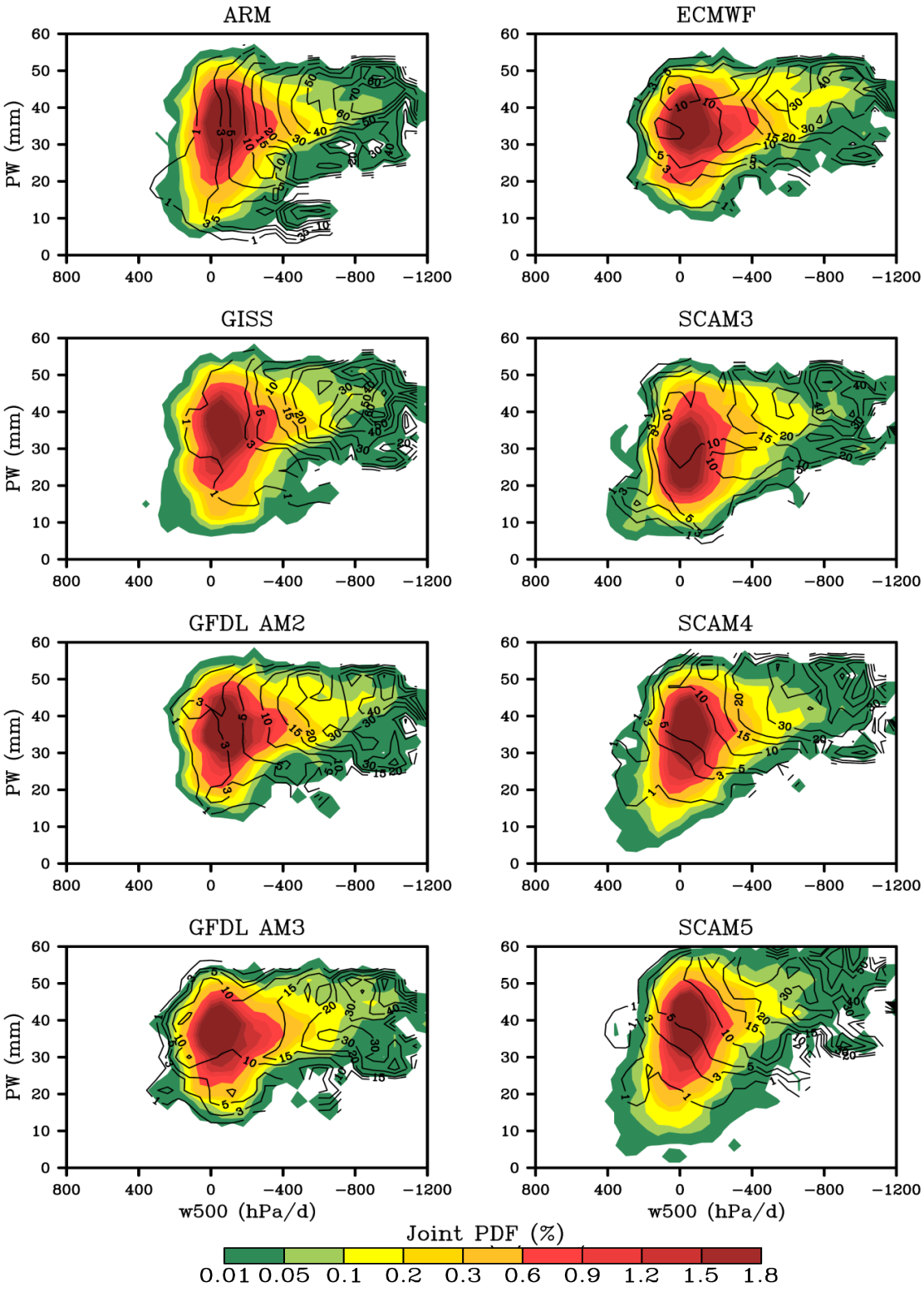

Figure S3: Same as in Figure 8 except for warm season.

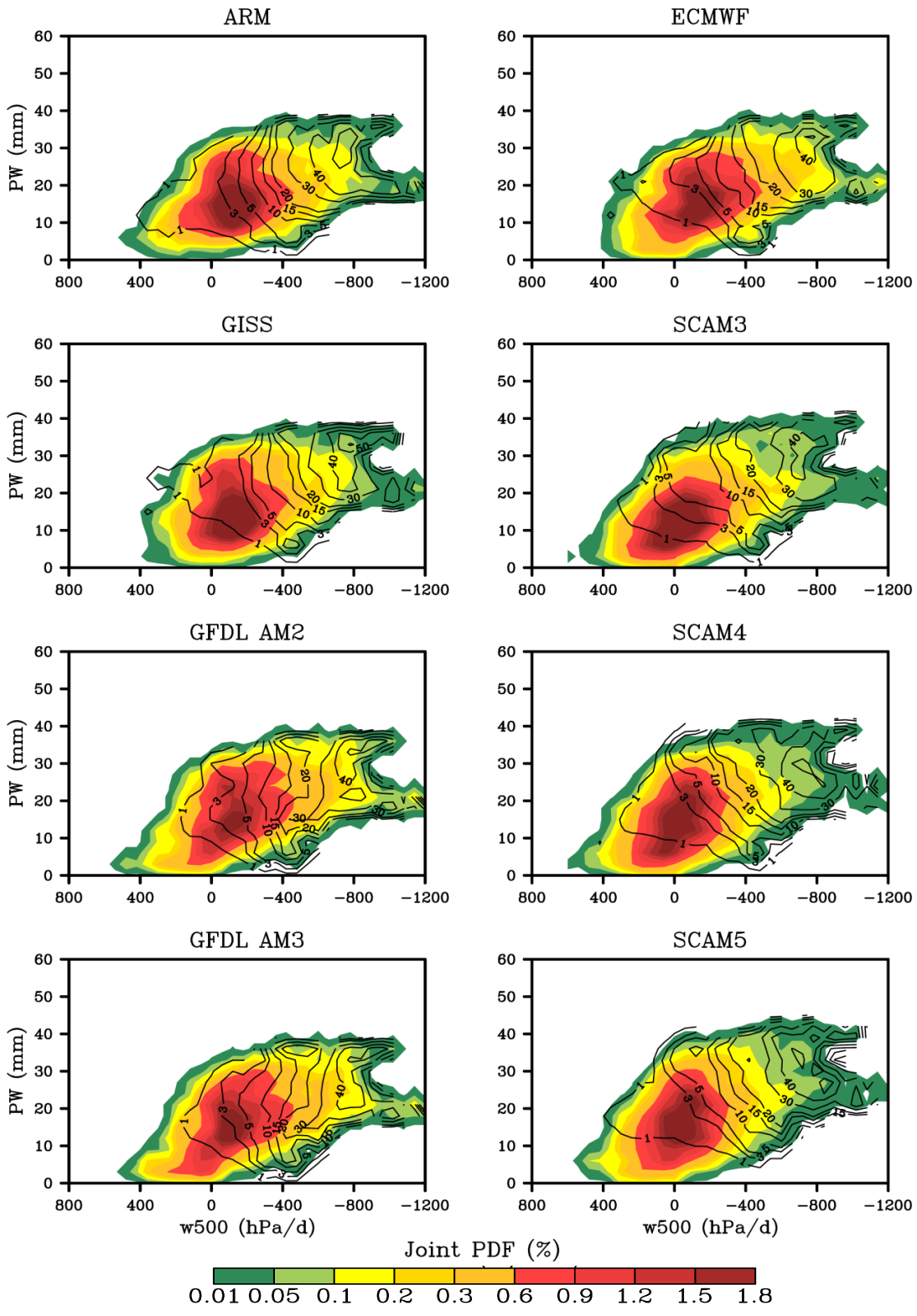

Figure S4: Same as in Figure 8 except for cold season.

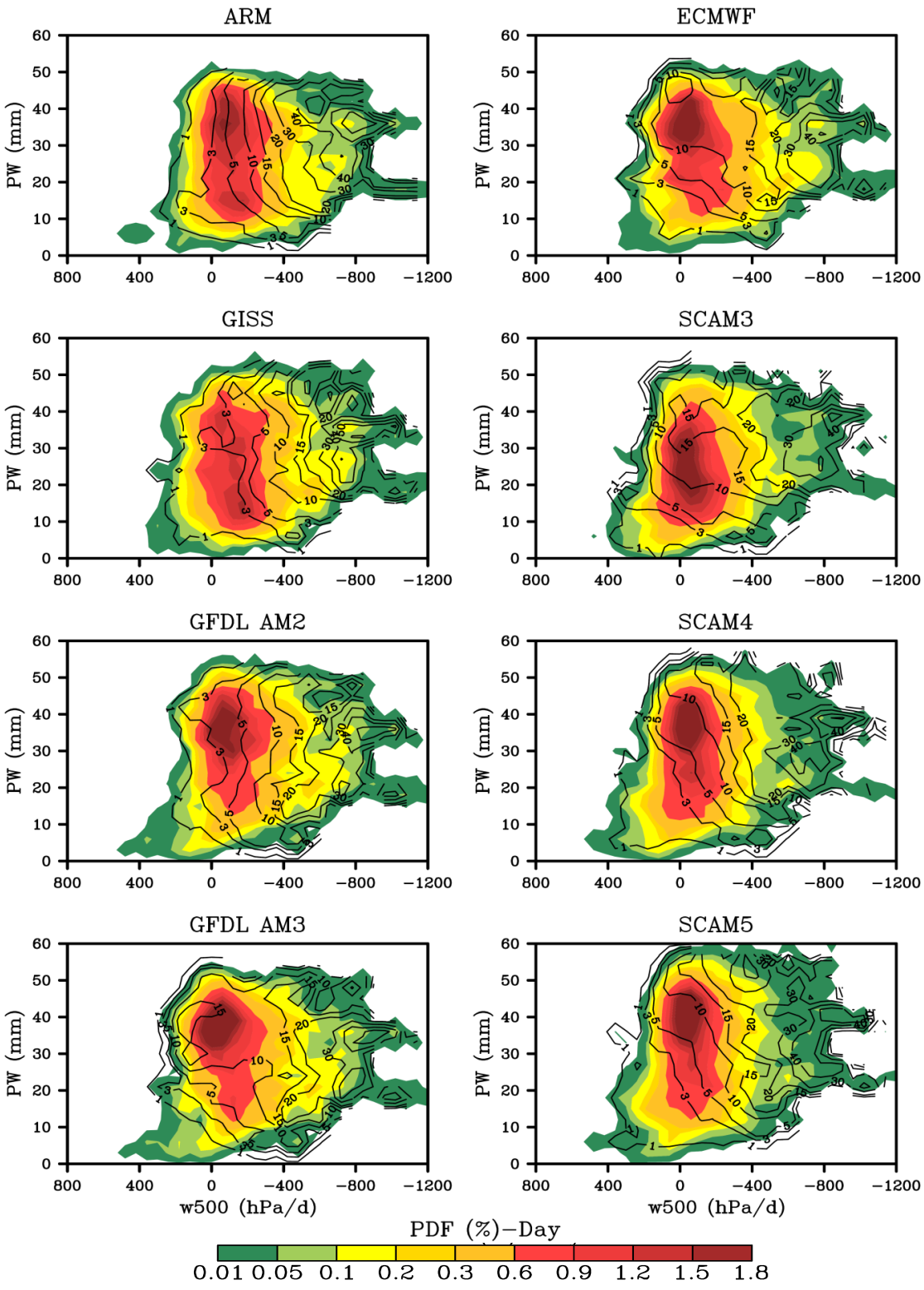

Figure S5: Same as in Figure 8 except for daytime.

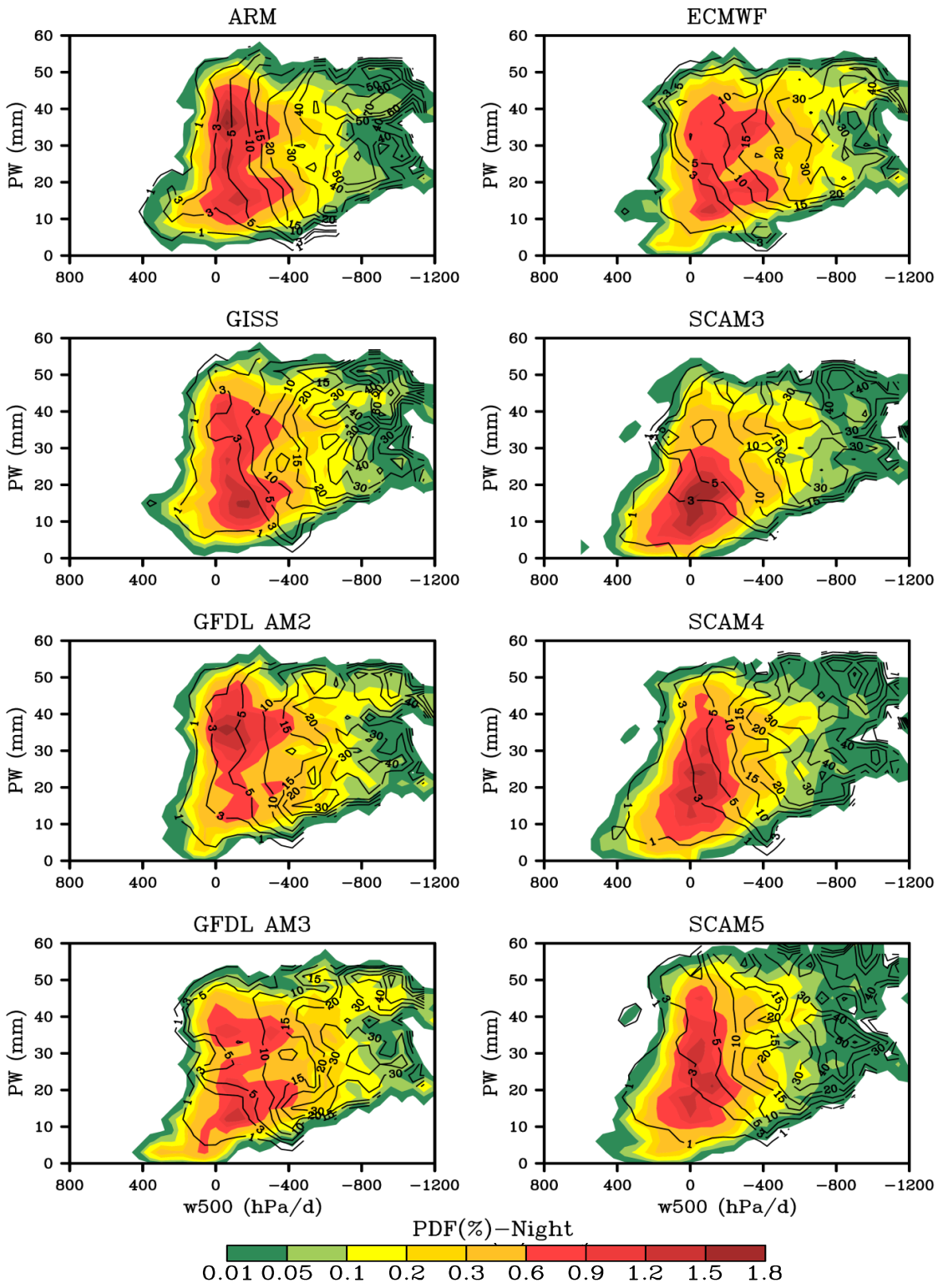

Figure S6: Same as in Figure 8 except for nighttime.

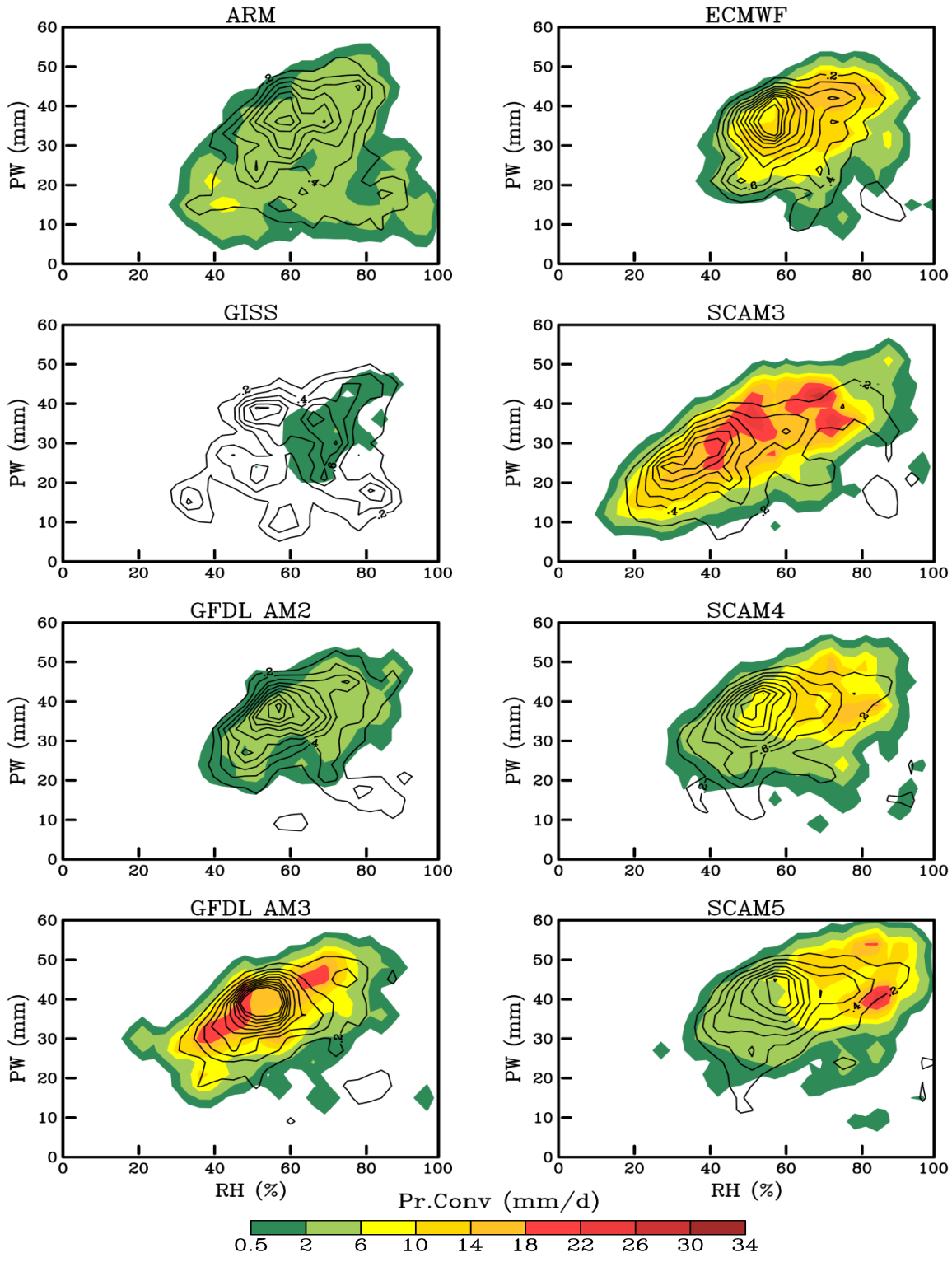

Figure S7: Same as in Figure 10 except for daytime.

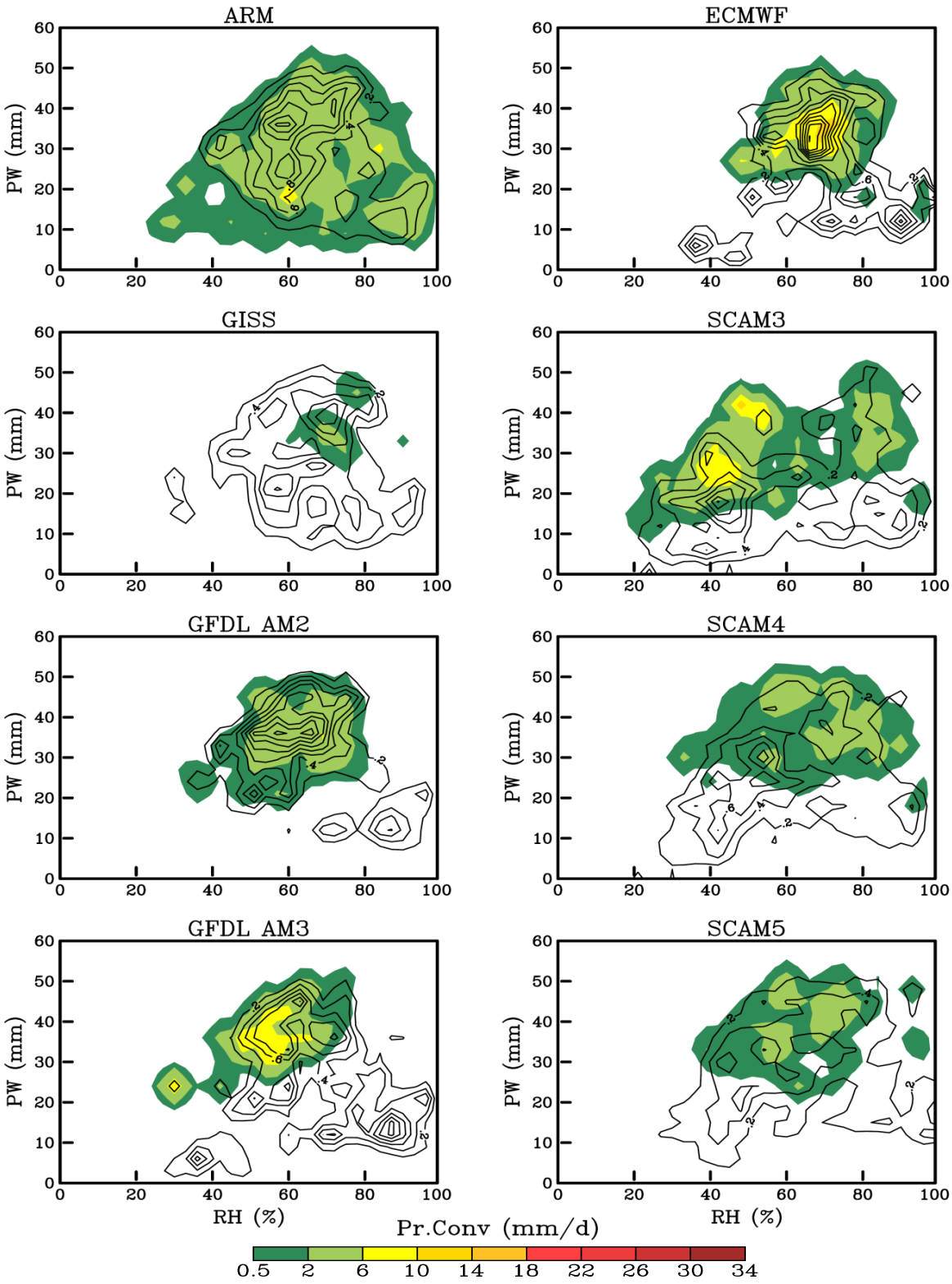

Figure S8: Same as in Figure 10 except for nighttime.